Research Square

Preprints are preliminary reports that have not undergone peer review.
They should not be considered conclusive, used to inform clinical practice,
or referenced by the media as validated information.

Identification of constitutive NK cell features associated with post-treatment control of SIV infection. The pVISCONTI study

Asier Saez-Cirion

asier.saez-cirion@pasteur.fr

Institut Pasteur https://orcid.org/0000-0003-2406-7536

Anais Chapel

Institut Pasteur

Luis Romero-Martin

Institut Pasteur

Caroline Passaes

Institut Pasteur https://orcid.org/0000-0002-0813-2521

Valérie Monceaux

Institut Pasteur https://orcid.org/0000-0002-8599-2146

Stevenn Volant

Institut Pasteur

Delphine Desjardins

Université Paris-Saclay, INSERM, CEA https://orcid.org/0000-0002-5820-3914

Adeline Melard

Institut Cochin https://orcid.org/0000-0003-1207-0201

Annie David

Institut Pasteur

Nathalie Dereuddre-Bosquet

CEA, Division of Immuno-Virology, Institute for Emerging Diseases and Innovative Therapies (iMETI)
https://orcid.org/0000-0001-6682-6313

Christine Rouzioux

APHP

Véronique Avettand-Fenoel

Université d'Orléans https://orcid.org/0000-0002-7022-2990

Michaela Muller-Trutwin

Institut Pasteur https://orcid.org/0000-0002-3854-2396

Roger Le Grand

Université Paris-Saclay, Inserm, CEA, Center for Immunology of Viral, Auto-immune, Hematological and Bacterial diseases (IMVA-HB/IDMIT), Fontenay-aux-Roses & Le Kremlin-Bicêtre, France
https://orcid.org/0000-0002-4928-4484

Article

Keywords:

Posted Date: February 27th, 2026

DOI: https://doi.org/10.21203/rs.3.rs-8789706/v1

License: This work is licensed under a Creative Commons Attribution 4.0 International License.
Read Full License

Additional Declarations: There is **NO** Competing Interest.

Version of Record: A version of this preprint was published at Nature Communications on August 22nd, 2026. See the published version at https://doi.org/10.1038/s41467-026-76699-7.

Identification of constitutive NK cell features associated with post-treatment control of SIV infection. The pVISCONTI study

Anaïs Chapel[1,2,*], Luis Romero-Martín[1,*], Caroline Passaes[1,2,&], Valérie Monceaux[1,2], Stevenn Volant[1], Delphine Desjardins[3], Adeline Melard[4], Annie David[2], Nathalie Dereuddre-Bosquet[3], Christine Rouzioux[5], Véronique Avettand-Fenoel[4,6], Michaela Müller-Trutwin[2], Roger Le Grand[3], Asier Saez-Cirion[1,2,#]

[1] Institut Pasteur, Université Paris Cité, Viral Reservoirs and Immune Control Unit, Paris, France.

[2] Institut Pasteur, Université Paris Cité, HIV, Inflammation and Persistence Unit, Paris, France.

[3] Université Paris-Saclay, CEA, INSERM, UMR1184, Immunology of Viral Auto-immune, Hematological and Bacterial diseases (IMVA-HB/ IDMIT Department), Fontenay-aux-Roses/Le Kremlin-Bicêtre, France.

[4] Université Paris Cité, INSERM, U1016; CNRS, UMR8104 Paris, France.

[5] Université Paris Cité, Paris, France.

[6] CHU d'Orléans, Orléans, France.

* The first two authors contributed equally to this work

[&]Current affiliation: Pasteur Fiocruz Center on Immunology and Immunotherapy, Eusébio, Ceará, Braz

Corresponding author: Asier Sáez-Cirión, asier.saez-cirion@pasteur.fr

Abstract

Post-treatment HIV controllers (PTC) offer a unique opportunity to uncover the determinants of durable remission after antiretroviral therapy (ART) interruption. Early ART initiation has been shown to favor this outcome, but the underlying immune mechanisms remain unclear. Recent reports suggest that natural killer (NK) cells may play a key role in post-treatment control of infection; however, a direct association with specific NK cell features has not been firmly established.

We used a recently reported model of post-treatment control of $SIVmac_{251}$ infection in Cynomolgus macaques (the pVISCONTI study) to analyze the constitutive and infection-induced characteristics of NK cells and their association with post-treatment viral control. Studying six PTC and six post-treatment non-controllers, we identified two NK cell subsets differing in the expression of NKG2A, NKp30, and NKp46, and which abundance prior to infection showed opposite associations with the outcome after ART interruption. $NKG2A^{high}$ NK cells lacking NKp30/NKp46 ($NKG2A^{high}NKp30^{-}NKp46^{-}$), shaped by the MHC background of the animals, were linked to improved post-treatment control. This subset displayed tissue-homing potential and preserved functionality despite infection, characterized by cytokine production and degranulation. Conversely, $NKG2A^{low}NKp30^{+}NKp46^{+}$ NK cells exhibited reduced cytotoxicity and elevated IL-10/IL-17A production, and their pre-infection levels were associated with higher viremia and larger viral reservoirs after ART interruption.

Our study indicates that constitutive NK cell features, preserved by early ART initiation, may provide a favorable immune environment for post-treatment control. These findings further identify the NKG2A axis as a potential target to improve outcomes after ART interruption.

Introduction

Despite the effectiveness of antiretroviral therapy (ART) in suppressing HIV replication, the virus cannot be eradicated from the organism, and most individuals experience rapid viral rebound following analytical treatment interruption (ATI). However, a rare subset of individuals, known as post-treatment controllers (PTC), durably maintain low level viremia after discontinuing ART. These individuals serve as important models for investigating the mechanisms underlying durable viral remission.

Several studies support that early and prolonged ART increases the likelihood of post-treatment control[1–4]. Further support comes from multiple meta-analyses of ATI studies, which show that the time to viral rebound correlates with the delay between HIV acquisition and ART initiation[5,6]. Although early treatment reduces the size of the viral reservoir[4,7], preserves mucosal immune cell populations[8] and immune response[9], it remains unclear whether a specific window of time exists to develop effective immune responses that would support long-term control after ATI. Notably, only a small proportion -approximately 6%, according to some studies[6]-of individuals treated early achieve post-treatment control, though definitions vary among cohorts.

Distinct features identified in PTCs include low levels of HIV DNA in peripheral blood mononuclear cells (PBMCs)[2,10], higher CD4+ nadir and CD4/CD8 ratio[6], lower T cell activation and exhaustion. Intact, replication competent, proviruses have been found in PTCs, pointing to a critical role of immune factors in these individuals[2,11,12]. However, post-treatment control is likely multifactorial, and the underlying mechanisms remain elusive.

We have recently identified an immunogenetic signature related to enhanced NK cell education via specific killer-cell immunoglobulin-like receptors (KIRs), which was highly prevalent among PTCs from the VISCONTI study and associated with higher probability of post-treatment control among people who started ART during primary infection[13]. This signature is typically accompanied by low HLA-E levels and elevated NK cell expression of NKG2A [14]. Other studies have reported the presence of NK cells with robust antiviral activities among PTCs[15,16]. These

findings point to a critical role for NK cells in maintaining viral suppression after ART discontinuation, although the links remain unclear.

NK cells are highly heterogeneous and participate in diverse immune defense mechanisms. In the context of HIV infection, several NK cell-mediated mechanisms have been proposed to contribute to viral suppression, including (1) direct and antibody-dependent cytotoxicity[17,18] (2) secretion of antiviral cytokines and chemokines that recruit other immune cells and inhibit viral replication[19], and (3) modulation of the adaptive immune response through dendritic cell (DC) regulation[20] or elimination of activated T cells[21,22].

In the non-pathogenic African green monkey model of SIV infection, NK cells upregulate CXCR5, migrate to mesenteric lymph nodes, and help preserve germinal center integrity and SIV-specific IgA levels[23]. Additionally, NK cells with adaptive features and increased HLA-E-restricted activity have been implicated in SIV control in peripheral lymph nodes[24]. Together, these observations underscore the central role of NK cells in both direct viral clearance and in orchestrating effective adaptive immunity while mitigating chronic immune activation.

Previous analyses of NK cells in the context of post-treatment HIV control have been limited to a period of well-established control, preventing the exploration of their implication before and during ART interruption. We recently implemented a model of SIVmac$_{251}$ infection of cynomolgus macaque (CyMs) to assess the impact of early (week 4 post-infection) versus late (week 24 post-infection) ART initiation on post-treatment control after 2 years of treatment (the p(rimate)VISCONTI study)[25] . The pVISCONTI study showed that early ART initiation strongly favored durable post-treatment SIV control in this model and provided a unique opportunity to explore longitudinally the underlying immune mechanisms.

Hereby, we study the role of NK cells in viral control after ART interruption by comparing the phenotype, function and dynamics of NK cells in six PTC macaques and six post-treatment non-controller (PTNC) macaques from the pVISCONTI study. We show that constitutive NK cell features, shaped before SIV infection, correlate with sustained post-treatment control and reduced

viral reservoir at the study endpoint. Moreover, we identified two opposing NK cell subsets that either negatively or positively influenced outcomes after ART interruption.

Material and Methods

Ethic statement

CyMs sourced from Mauritius were housed at the Infectious Disease Models and Innovative Therapies (IDMIT) center (CEA site, Fontenay-aux-Roses, France). All nonhuman primate research at IDMIT adhered to French national regulations under the oversight of veterinary inspectors (CEA Permit No. D92-032-02) and met the Office for Laboratory Animal Welfare's care and use standards (Assurance Nos. A5826-01 and F20-00448). Procedures complied with European Directive 2010/63 (Recommendation No. 9). The pVISCONTI study received approval from the Comité d'Éthique en Expérimentation Animale du CEA (statement A15 035) and was registered with the French Ministry of Education and Research (No. 2453-201510271332361v3). Animal handling, viral inoculations, and sample collection occurred under ketamine chlorhydrate sedation (Imalgene 1000®, 10 mg/kg IV, Merial). Tissues were obtained during follow-up and at necropsy. Euthanasia followed initial ketamine sedation with an intravenous bolus of sodium pentobarbital (Doléthal, 180 mg/kg, Laboratoire Vetoquinol).

Animal and experimental conditions

This study includes a subgroup of 12 male CyMs (6 classified as PTCs and 6 as PTNCs) from the pVISCONTI study[25] (median age = 4.73 years, IQR = 0.93 years), which were dedicated to in-depth immunological characterization (Table S1). The conclusions are not sex-based. Infection was performed at an animal infectious dose $(AID)_{50}$ of 1000 by intravenous inoculation with uncloned $SIVmac_{251}$ kindly provided by Anne-Marie Aubertin (Université Louis Pasteur, Strasbourg, France)[26].

ART containing emtricitabine (FTC, 40mg/kg, Gilead), dolutegravir (DTG, 25mg/kG, ViiV Healthcare) and tenofovir-disoproxil-fumarate (TDF, 5.1 mg/kg, Gilead) was coformulated as a daily subcutaneous injection. ART was initiated either at week 4 (n=6) or week 24 (n=6) and was continued for 24 months before following ATI. Animals were classified as PTC if they reached at

least one pVL<400 SIV RNA copies/mL (similar to the viral load threshold for PTCs in the HIV-1 VISCONTI cohort[2]) after viral rebound or if they did not experience viral rebound. The endpoint was 48 weeks after ATI, except for PTNC showing progression to disease before this time. All animals were monitored for at least 6 months post ATI.

Blood collection and processing

Venous blood was drawn into either Vacutainer Plus Plastic K3EDTA Tubes or Vacutainer CPT Mononuclear Cell Preparation Tubes containing sodium heparin (BD Biosciences). Plasma was isolated from the K3EDTA by centrifugation for 10min at 480g. PBMCs were isolated from the CPT tubes following the manufacturer's instructions (BD Biosciences), and residual red blood cells were lysed in ammonium-chloride-potassium (ACK) buffer (0.15 M NH_4Cl, 10 mM $KHCO_3$, 0.1 mM EDTA, pH 7.4).

Tissue collection and processing

Samples from axillary or inguinal lymph nodes (peripheral pLNs), bone marrow (BM), and bronchoalveolar lavage (BAL) were collected over time. At necropsy, the spleen, mesenteric lymph nodes (mLNs), colon, and liver were also harvested. All tissues were kept in RPMI medium at 2–8 °C. Lymph node cells were obtained by mechanically dissociating the nodes with a gentleMACS Dissociator (Miltenyi Biotec), filtering the suspension through a 70 µm mesh, then lysing red blood cells in ACK buffer. Bone marrow cells were isolated using Lymphocyte Separation Medium (Eurobio Scientific) diluted to 90% in DPBS, centrifuged for 20 min at 350 × g, and residual erythrocytes removed by ACK lysis. Spleen cells underwent a similar process: mechanical disruption in RPMI with the gentleMACS Dissociator, density separation as for BM cells, and ACK-mediated red cell lysis. For colonic lymphocytes, mucosa from roughly 10 cm of colon was extensively washed in PBS and R10 (RPMI with 10% fetal calf serum and penicillin/streptomycin), then digested for 45 min with collagenase II before mechanical

dissociation; lymphocytes were finally isolated over a 67/44 Percoll gradient (Sigma-Aldrich). Liver tissue was likewise dissociated mechanically, the suspension sequentially filtered through 300 µm, 100 µm, and 70 µm meshes, and lymphocytes recovered via an OptiPrep gradient (Sigma-Aldrich).

Quantification of plasma viral load

Longitudinal monitoring of plasma viral load was performed by quantitative RT-PCR (limit of detection = 12.3 SIV RNA copies/mL). Viral RNA was prepared from 100 µL of cell-free plasma. The assay was performed using a SuperScript III Platinum One Step-Step qRT-PCR Kit (Thermo Fisher Scientific) with a CFX96 Touch Real-Time PCR Detection System (Bio-Rad). Each tube contained 12.5 µL of 2× reaction mixture, 0.5 µL of RNaseOUT (40 U/µL), 0.5 µL of Superscript III Reverse Transcriptase/Platinum Taq DNA Polymerase, 1 µL of each primer (125 µM), 0.5 µL of the fluorogenic probe (135 µM), and 10 µL of eluted RNA. Primer/probe sequences were designed to amplify a region of the $SIVmac_{251}$ gag gene. The forward (F) primer sequence was 5′-GCAGAGGAGGAAATTACCCAGTAC-3′ (24 bp), and the reverse (R) primer sequence was 5′-CAATTTTACCCAGGCATTTAATGTT-3′ (25 bp). The probe sequence was 5′-FAM-TGTCCACCTGCCATTAAGCCCGA-BHQ1-3′ (23 bp). This probe had a fluorescent reporter dye, FAM (6-carboxyfluorescein), attached to its 5′ end and a quencher, BHQ1 (black hole quencher 1), attached to its 3′ end (TaqMan, Applied Biosystems). Samples were heated for 30 minutes at 56 °C and 5 minutes at 95 °C, followed by 50 thermocycles, each comprising 15 seconds at 95 °C and 1 minute at 60 °C.

Quantification of SIV-DNA

Total DNA was extracted from purified $CD4^+$ T-cells from PBMC, pLN or mLN cells with an AllPrep DNA/RNA Mini kit (Qiagen). Two or three samples were used per tissue and disrupted separately with a MagNA Lyser (GmbH, Roche Diagnostics, Brussels, Belgium) to minimize the

differences in viral distribution within an organ. The total SIV-DNA was quantified by ultrasensitive real-time PCR targeting the gag region[27].The cycling conditions were 2 minutes at 50 °C and 10 minutes at 95 °C followed by cycles at 95 °C for 15 seconds and 60 °C for 1 minute. The limit of detection was 1 copy/PCR. To normalize SIV-DNA per million cells, the CCR5 gene was quantified by real-time PCR with the same cycling conditions described above (forward primers: an equimolar mix of the primers 5′-CAACATGCTGGTCGATCCTCAT-3′ and 5′-CAACATACTGGTCGTCCTCA TCC-3′, reverse primer: 5′-CAGCATAGTGAGCCCAGAAG-3′, probe: 5′-HEX-CTGACA TCTACCTGCTCAACCTG-BHQ1-3′). For both PCRs, the reaction volumes were 50 µL, containing 25 µL of 2× qPCR Mastermix Plus (Eurogentec, Seraing, Belgium), 0.4 µM each primer and 0.2 µM probe. SIV-DNA levels were reported as copies per 10^6 $CD4^+$ T cells or as threshold values when the SIV-DNA level was under the detection threshold or SIV-DNA was not detected.

Analysis of NK cell phenotype

NK cell phenotype was assessed longitudinally using fresh PBMCs and tissue cell suspensions. Cells were first stained with the LIVE/DEAD Fixable Aqua Dead Cell Stain Kit (Thermo Fisher Scientific) and then stained for surface expression of: anti-CD3 V450 (Clone SP34-2, BD Biosciences), anti-CD14 V450 (clone M5E2, BD Biosciences), anti-CD20 V450 (Clone L27, BD Biosciences), anti-HLA-DR Pacific Blue (clone G46-6, BD Biosciences), anti NKG2A FITC (Clone REA110, Miltenyi), anti-NKp46 PC7 (Clone BAB281, Beckman Coulter), anti-CD8 PerCP-Vio700 (Clone BW135/80, Miltenyi), anti-CD56 PE-CF594 (Clone NCAM16.2, BD Biosciences), anti-NKp30 PE (Clone AF29-4D12, Miltenyi), anti-CD69 APC-Cy7 (Clone FN50, Biolegend), anti-CD16 AF700 (Clone 3G80, Biolegend), anti-NKp80 APC (Clone 4A4.D10, Miltenyi). To evaluate the homing potential, cells were stained with anti-CD3, anti CD14, anti-CD20, anti-HLA-DR, anti-NKG2A and anti-NKp80 as above, and anti-CXCR4 PECy7 (Clone 12G5, BD), anti-CXCR3 PerCP-Cy5.5 (Clone 1C6, BD), anti-CCR7 PE-Dazzle594 (Clone G043H7, BioLegend), anti-CXCR6 PE (Clone 568, R&D), anti- α4/β7 APC-Fire750 (Clone

FIB504, BioLegend) and anti-CXCR5 APC-R700 (Clone RF8B2, BD). Cells were then fixed with PFA 4% solution and acquired using an LSRII flow cytometer (BD Biosciences). NK cells were gated as Live- Lineage- (CD3-CD14-CD20-HLADR-)NKp80+[28,29].

Analysis of NK cell function

NK cells were isolated from 10 million cryopreserved PBMC by negative magnetic bead separation using a custom NHP NK cell isolation kit (Miltenyi) (Fig. S1). After 2h of resting at 37ºC, 200.000 NK cells were seeded in a 96-well culture plate with/without 50.000 K562 target cells (effector:target ratio = 2:1) for 4h in the presence of Brefeldin A (5 µg/mL, Sigma-Aldrich) and GolgiStop (1 µL/mL, BD Biosciences) and anti-CD107a BV421 (Clone H4A3, Biolegend). Viability was determined by the Fixable Viability Stain 570 (BD Biosciences). Extracellular staining was performed as described above including anti-FasL BUV737 (Clone NOK-1, BD Biosciences). Cells were fixed and permeabilized (Fix&Perm Cell Permeabilization Kit, Thermofisher) and stained anti-CCL4 AF350 (Clone 24006, R&D), anti-TNF-α BV786 (Clone MAb11, Biolegend), anti-IL-10 BV650 (Clone JES3-9D7, BD Biosciences), anti-Granzyme-B BV510 (Clone GB11, Biolegend), anti-Granzyme K PerCP-eFluor710 (Clone G3H69, Thermofisher), anti-IL-17A PE-Vio615 (Clone CZ8-23G1, Miltenyi) and anti-IFN-γ Spark NIR 685 (Clone 4S.B3, Biolegend). Samples were acquired in a Sony ID7000 spectral analyzer.

Data analysis, statistics and visualization

Flow cytometry data was analyzed with OMIQ software (Dotmatics). Normalization was performed on the longitudinal staining by CyCombine in order to minimize batch effects. High-dimensional data was analyzed with Qlucore software. Graphs and statistical analysis were performed using Prism v10.4 (GraphPad Software) or R. χ^2 analysis was used to evaluate absolute frequencies of MHC variants. Multiple comparisons were performed by two-way ANOVA with *post-hoc* false discovery rate correction (FDR). Correlation analysis was performed by non-

parametric Spearman rank test. Statistical significance was established at p-value < 0.05 and q-value < 0.1. Flourish was used for data visualization.

Results

The presence of specific NK cell subsets since baseline associated with outcome after treatment discontinuation

The objective of this study was to evaluate the role of NK cells in the achievement of SIV control following treatment discontinuation. We studied 12 animals from the pVISCONTI study (Table S1). All macaques except one experienced a viral rebound after treatment interruption ($7.18x10^6$ [$6.19x10^6$, $11.46x10^6$] median and IQR peak SIV RNA copies/mL). However, 5 macaques (4 treated at W4 post infection, p.i., and 1 treated at W24 p.i.) rapidly decreased those levels. In total, 6 animals maintained stable and controlled pVL after ATI (68 [24, 89] SIV RNA copies/mL at last follow up), achieving the status of post-treatment controller (PTC). The other 6 macaques (1 treated at W4 p.i. and 5 treated at W24) maintained high pVL ($2.41x10^4$ [$1.01x10^4$, $4.37x10^4$] SIV RNA copies/mL at last follow up) and were defined as post-treatment non-controllers (PTNC).

There were no differences in pVL between PTC and PTNC during the acute infection (Fig. 1A), and all animals had indetectable pVL at the time of ATI. In contrast, a small difference was observed in $CD4^+$ T-cells-associated total SIV-DNA levels pre-ATI (p-value = 0.0080). The frequency of cells carrying SIV-DNA strongly increased in PTNC after ATI and higher levels than in PTCs were found in CD4+ T-cells from PBMC, peripheral and mesenteric lymph nodes at the end of the study (p-value = <0.0001) (Fig. 1B).

NK cell phenotype was longitudinally analyzed in fresh samples in blood at baseline, acute infection, during ART and after ATI. NK cells were defined as $CD3^-CD14^-CD19^-NKp80^+$[28,29] (Fig. S2) and dimensional reduction was set at 4000 NK cells/sample (total > 870.000 cells considered) by Fit-tSNE. Fourteen clusters were identified in an unsupervised manner by FlowSOM (Elbow Plot determination) based on the expression of CD16, CD56, CD69, CD8, NKG2A, NKp30 and NKp46 (Fig. 1C). Overall, the distribution of the NK cell clusters remained relatively stable before ATI, except for a decrease in cluster 12 (CD16+CD56+CD69+) at day 28 p.i. (p<0.0001) and maintained after 2 years of ART (p=0.0001) and an expansion of cluster 9 (CD16+CD56-) at

the end of the ART period (p=0.004), which recapitulates previous observations in the context of HIV/SIV infections[30] (Fig. 1D).

To assess whether, individually, NK cell distribution at different timepoints might have influenced outcome after ATI, we performed a correlation analysis between the proportion of the 14 defined clusters and three virological parameters: the cumulative plasma viral load (as determined by the area under the curve, AUC) during viral rebound (first 35 days) or extended follow up (165 days) after ATI, and the cell-associated total SIV-DNA in the mLN at the end of the study. The frequency of four clusters (Clusters 1, 3, 4 and 5) at the baseline, at day 28 p.i. and/or before ATI showed negative correlations with cumulative viremia and/or viral reservoir, pointing to a beneficial impact of the presence of these cells on the level of viral control after ATI. Conversely, three clusters (Clusters 6, 7 and 8) showed positive correlations with the same virological parameters (Fig. 1E). Notably, all the clusters associated with better post-treatment control were characterized by a high expression of NKG2A and low to intermediate expression of NKp30 and/or NKp46. In contrast, clusters negatively linked to viral control showed low levels of NKG2A and medium to high levels of NKp30 and NKp46 (Fig. 1F). These findings suggest that the intrinsic characteristics of NK cell populations, already present at the baseline before infection, may influence the ability to control viral rebound after interruption of 2 years-long ART.

Opposing effects of NKG2A^{high}NKp30^{-}NKp46^{-} and NKG2A^{low}NKp30^{+}NKp46^{+} cells overtime on the outcome after treatment discontinuation

The unsupervised analysis revealed diametrical opposed effects of cells subsets with a NKG2A^{high}NKp30$^{-/low}$NKp46$^{-/low}$ vs NKG2A^{low}NKp30$^{low/high}$NKp46$^{low/high}$ phenotypes. We therefore manually defined NKG2A^{high}NKp30^{-}NKp46^{-} and NKG2A^{low}NKp30^{+}NKp46^{+} NK cells to further explore their dynamics and potential implication on post-treatment control (Fig. 2A). These NK cell populations followed different dynamics following infection (Fig. 2B and Fig S3). The proportion of NKG2A^{high}NKp30^{-}NKp46^{-} cells decreased following infection in all animals

during the first weeks of primary infection. ART initiation appeared to stop this drop but did not restore the frequency of these cells, even after 2 years of treatment. In contrast, the frequency of NKG2A^{low}NKp30^{+}NKp46^{+} cells increased during acute infection but frequencies were similar to baseline after two years on ART (Fig. S3). Of note, PTC tended to have a higher proportion of NKG2A^{high}NKp30^{-}NKp46^{-} cells since the baseline than PTNC (Figure 2B), a difference that was maintained until the time of ART interruption. At this time PTCs were in contrast characterized by a lower frequency of NKG2A^{low}NKp30^{+}NKp46^{+} cells than PTNC. Accordingly, a strong negative correlation was found between baseline NKG2A^{high}NKp30^{-}NKp46^{-} cells and the cumulated plasma viral loads during viral rebound (days 0-35 post ATI) (ρ = -0.8161, p-value = 0.0019) and extended follow-up (days 0-165 post ATI) (ρ = -0.7426, p-value = 0.0075), or with the SIV reservoir in the mLN at Euthanasia (ρ = -0.7986, p-value = 0.0027) (Fig. 2C). Of note, negative correlations with the cumulated viremia after ATI (especially during viral rebound) and/or the cell-associated SIV-DNA levels in mLN at the end of the study were consistently found when we considered the frequency of NKG2A^{high}NKp30^{-}NKp46^{-} cells present during acute infection (days 0, 3, 14 and 27), after ART initiation (weeks 24, 52, 78 and 100) and following ATI (weeks 1, 4) (Fig. 2C). On the contrary, positive correlations were found between the frequency of NKG2A^{low}NKp30^{+}NKp46^{+} at baseline and at multiple time points during acute infection, after ART initiation and upon ATI with the cumulated viremia after ATI and the viral reservoir in mLN at the end of the study.

These data comforted the unsupervised analyses and identified two NK cell subsets which frequency at the time of infection—and their trajectories throughout acute infection, ART, and ATI—might differently influence the ATI outcome. A higher baseline frequency and sustained levels of NKG2A^{high}NKp30^{-}NKp46^{-} cells were associated with reduced viral rebound and better post-treatment control, while elevated levels of NKG2A^{low}NKp30^{+}NKp46^{+} cells were associated with higher viremia and SIV reservoir after ART interruption. Hereby, an intrinsic composition of NK cell subpopulations and the dynamics during the infection may decisively determine the capacity to contain the viral rebound after treatment discontinuation.

315

316 Opposed tissue dynamics for NKG2A^{high}NKp30^{-}NKp46^{-} and NKG2A^{low}NKp30^{+}NKp46^{+} cells
317 during acute infection and treatment

318 The NK cell subsets of interest (NKG2A^{high}NKp30^{-}NKp46^{-} and NKG2A^{low}NKp30^{+}NKp46^{+}) were
319 not restrained to the blood and we found them in multiple tissues, including the spleen, the liver,
320 bronchoalveolar lavage (BAL) and the gut, at the end of the study (Fig. S4). We evaluated their
321 distribution longitudinally in two different lymphoid tissues (pLN- and bone marrow -BM-).
322 Consistent with the dynamics of circulating NKG2A^{high}NKp30^{-}NKp46^{-} cells, there was a sharp
323 decrease in the frequency of this cell subset in both lymphoid tissues during the acute infection
324 (Baseline vs Before ART, p-value = 0.008 and 0.0012 for pLN and BM respectively). Levels
325 recovered after ART reaching basal levels in pLN but not in BM (p=0.0351) (Fig. 3A).
326 NKG2A^{low}NKp30^{+}NKp46^{+} cells followed opposite dynamics (Fig. 3B) increasing following
327 infection in both pLN and BM (p-value < 0.0001). Their frequency decreased after 2 years of
328 ART to almost-basal levels in pLN but remained elevated in BM (p-value = 0.0192) (Fig. 3B).

329 As in the case of circulating cells, the baseline frequency of NKG2A^{high}NKp30^{-}NKp46^{-} cells in
330 BM correlated negatively with the cumulated viremia after ATI (days 0-35 and 0-165), and their
331 frequency before ART in pLN and BM showed a negative correlation with both cumulated
332 viremia after ATI and SIV reservoir levels in blood and mLN at the end of the study. In contrast
333 NKG2A^{low}NKp30^{+}NKp46^{+} cells in pLN showed positive correlations with cumulated viremia
334 (days 0-35 and 0-165) and with SIV reservoir in PBMC and mLN at the end of the study.

335 Our results showed contrasting dynamics of NKG2A^{high}NKp30^{-}NKp46^{-} cells (which decreased
336 during acute infection) and NKG2A^{low}NKp30^{+}NKp46^{+} cells (which accumulated during the same
337 period) which were more marked in pLNs and BM than in blood. Of note, higher tissue levels of
338 NKG2A^{high}NKp30^{-}NKp46^{-} and lower levels of NKG2A^{low}NKp30^{+}NKp46^{+} were associated with
339 better viral control after ART interruption, mirroring the results found in blood.

340

NKG2A^{high}/NKG2A^{low} subsets are constitutive in each animal and are partly determined by their immunogenetic background

The NK cell subsets of interest were characterized by different expression levels of NKG2A, NKp30 and NKp46. The overall expression of NKp30 and NKp46 on NK cells was modulated by SIV infection and treatment. A reduction in the expression of NKp46 was observed at the end of the ART period, while NKp30 expression on NK cells increased during primary infection but returned to baseline levels after 2 years of ART. Overall, lower levers of NK cells expressing NKp30 were observed in PTCs at baseline (p-value = 0.029) and at the time of ART interruption (p-value = 0.0197) when compared to non-PTCs (Fig. S5).

In contrast to the other markers, the frequency of NKG2A^{high} NK cells remained stable during the complete follow-up. However, different constitutive levels were found among the macaques at the baseline: while all animals presented a NKG2A^{low} NK cell population, four of the animals studied here had negligeable levels of NKG2A^{high} NK cells. This different constitutive presence of NKG2A^{high} cells was observed in blood and, at different rates, in lymphoid tissues, including pLN, mLN, BM and spleen (Fig. 4A), and non-lymphoid tissues as liver, gut and BAL (Fig. 4B). We therefore evaluated possible determinants of the presence or absence of NKG2A^{high} NK cell subsets. To increase the statistical power, we analyzed samples from 16 additional non-infected macaques. In total, seventeen macaques were characterized by the presence of NKG2A^{high} NK cells, while eleven (termed NKG2A^{low}) did not carry the NKG2A^{high} NK cell subset. The abundance of NKG2A^{high} cells did not correlate with the age (ρ = -0.01674, p-value = 0.9326) nor the weight (ρ = -0.2251, p-value = 0.9326) of the animals (Fig. S6A). Accordingly, we did not observe any correlation either between the frequency of NKG2A^{high}NKp30^{-}NKp46^{-} cells and age (ρ = 0.08, p-value = 0.69) or the weight (ρ = 0.07, p-value = 0.71) (Fig. S6B).

We then explored the potential impact of the immunogenetic background on the constitutive presence of NKG2A^{high} cells. Due to their restricted diversity, Mauritian CyMs can be classified in a limited number of haplotypes based on microsatellite genotyping and allele-specific PCR[31]. We found the M1 (p-value = 0.0491) and M5 haplotypes (p-value=0.0325) were more frequent

among animals with the NKG2A^{low} profile, while the M3 haplotype (p-value = 0.0238) was more frequent in macaques with the NKG2A^{high} profile (Fig. 4C). We further explored whether these differences could be linked to specific microsatellites in the MHC region that defined the haplotypes. We found that the presence of the 277/278 alleles of the D6S2793 microsatellite, located within the MHC-B gene cluster[32], was significantly higher in macaques with a NKG2A^{low} profile (p-value = 0.0161). In contrast, we observed a trend for 145/146 alleles in the D6S2704 microsatellite, located between the MHC-A and MHC-B region, to be more frequent among macaques with the NKG2A^{high} phenotype (p-value=0.054). When combined, the presence of the 277/278+ D6S2793 allele in absence of 145/146- D6S2704 allele was much higher in NKG2A^{low} macaques (p-value=0.0033), while the opposite (277/278- 145/146+) was observed exclusively in animals with the NKG2A^{high} profile (p-value=0.0233) (Fig. 4D). We did not observe any significant difference regarding other alleles.

Overall, our results indicate that the presence or absence of NKG2A^{high} cells, associated with enhanced post-treatment control, might be constitutively influenced by the MHC-class I related immunogenetic background of the animals, mirroring the previous observations of NKG2A expression in humans[14].

Homing potential of NKG2A^{high} and NKG2A^{low} cells before ATI correlates with post-treatment control

The different relative distribution of NKG2A^{high} and NKG2A^{low} cell subsets in tissues suggest that these cells may possess different trafficking capacities. We therefore analyzed the expression of various homing markers in NKG2A^{high} and NKG2A^{low} NK cells in blood prior to ATI (Fig. S7). No significant differences were found regarding the individual expression of homing markers in each subset (Fig. 5A). Dimensional reduction was set at 4000 NK cells/sample by Fit-tSNE. Twenty clusters were identified in an unsupervised manner by FlowSOM (Elbow Plot determination) based on the expression of NKG2A and homing markers (Integrin α4β7, CXCR5,

CXCR6, CCR7, CXCR3 and CXCR4) (Fig. S8). Six clusters (4, 8, 9, 11, 13 and 20, Fig. 5B) showed significant positive or negative correlations with either the cumulated viremia after ATI or the SIV DNA levels in PBMC, pLN or mLN at the end of the study. Clusters 9, 11 and 20 were negatively correlated with cumulated viremia or the viral reservoir after ATI, whereas clusters 4,8 and 13 were positively correlated with these virological markers. Notably, all NK cell subsets associated with improved viral control after ATI corresponded to NKG2A^{high} cells expressing varying combinations of homing markers (Cluster 9: α4β7, CXCR5, CCR7, CXCR3, CXCR4; Cluster 11: α4β7, CXCR5, CXCR6, CCR7, CXCR3 and CXCR4; Cluster 20: CXCR6 and CXCR3) (Fig. 5C). In contrast, all clusters that positively correlated with markers of viremia and viral reservoir were composed of cells with intermediate or low levels of NKG2A that lacked homing markers (Fig. 5C).

These findings suggest that NK cells associated with post-treatment control are characterized both by NKG2A^{high} expression and homing potential, indicating that the capacity of NKG2A^{high} cells to localize in tissues may contribute to the containment of the viral rebound following ATI.

Functional profiling of distinct NKG2A^{high} and NKG2A^{low} NK cell subsets

Because of their strong positive and negative association with viral control after ATI, we hypothesized that NKG2A^{high}NKp30^{-}NKp46^{-} and NKG2A^{low}NKp30^{+}NKp46^{+} cells may have different functional capacities. We therefore measured at baseline, at week 52 after treatment initiation, and after ATI, the basal content of cytotoxic molecules in NK cells, and their capacity to release these molecules and several soluble factors after 4h culture with target cells (Fig. S9).

Overall, the NKG2A^{low} cells exhibited higher cytotoxic potential compared to NKG2A^{high} cells (as shown by higher expression of perforin, granzymes B and K in basal conditions) (Fig. 6A). However, the NKG2A^{low}NKp30^{+}NKp46^{+} cells carried less frequently perforin and Granzyme K, and had lower Granzyme B content, indicating that these cells represent a specific and comparatively less cytotoxic subset within the NKG2A^{low} population. NKG2A^{high}NKp30^{-}NKp46^{-}

and the broader NKG2A^{high} cells displayed relatively similar cytotoxic profiles, characterized by lower frequencies of Granzyme B^{high}/Granzyme K^{+} cells. In contrast, upon co-culture with target cells, NKG2A^{high} and NKG2A^{high}NKp30^{-}NKp46^{-} cells showed a higher capacity to degranulate and to produce TNF-α than NKG2A^{low} and NKG2A^{low}NKp30^{+}NKp46^{+} cells (Fig. 6B), which were characterized, in particular the latter, by the production of higher levels of IL-17A and IL-10 in response to target cells (Fig. 6C). The different functional profiles of the NK cell subsets were defined since the baseline and no major changes were observed at the three timepoints analyzed (Baseline, week 52 on ART or week 4 after ATI) except a trend for further loss of granzyme B and perforin content in NKG2A^{low}NKp30^{+}NKp46^{+} upon infection when compared to the total NKG2A^{low} compartment (Fig. 6D).

Our analysis identified profound functional differences between the NKG2A^{high} and the NKG2A^{low} compartments, corresponding to cytokine-producing and cytotoxic NK cells, respectively. Moreover, NKG2A^{low}NKp30^{+}NKp46^{+} cells showed, since the baseline, decreased cytotoxic potential and elevated capacity to produce IL-17A and IL-10 in response to target cells, distinguishing them from the broader NKG2A^{low} population, and this dysfunctionality was exacerbated by infection. In contrast, NKG2A^{high}NKp30^{-}NKp46^{-} NK cells were highly reactive and their functionality was not impacted by infection.

Discussion

In this study we have identified two NK cell subsets which relative abundance in CyMs before SIVmac251 infection was associated with the outcome of ART interruption over 2 years later. We exposed genetic influences, phenotype, trafficking potential and effector functions of these cell subsets that may help to understand the factors underlying post-treatment control of SIV infection in this model. Our results suggest that constitutive characteristics of NK cells influence the acquisition of PTC status.

The two NK cell subsets characterized here differ in their expression of NKG2A, NKp30, and NKp46, and show opposite associations with post-treatment control. Notably, NK cells expressing high levels of NKG2A were associated with improved post-treatment control. NKG2A is an inhibitory receptor, typically expressed on immature NK cells, that dampens NK cell activity upon interaction with its ligand, MHC-E, on target cells. However, NKG2A contributes to NK cell education, and both its expression level and the functional reactivity of NKG2A+ NK cells are influenced by leader peptides from conventional MHC class-I molecules, which modulate MHC-E surface expression. Intriguingly, the presence of NK cells expressing high levels of NKG2A was restricted to a subset of animals in the study. This pattern appeared to be shaped by the MHC background of the animals. Indeed, the absence of MHC M1 and/or M5 haplotypes, or the presence of M3, was associated with the detection of the NKG2A^{high} NK cell subset. We further traced this influence to specific allelic variants within two microsatellite loci in the MHC class-I region, although a mechanistic link remains to be formally established. It is worth noting that we have recently identified an immunogenetic fingerprint (HLA-B*35 Bw4TTC2) that is overrepresented among HIV-1 PTC from the VISCONTI cohort[13]. This genotype is associated with NK cell education and characterized by homozygosity for a threonine at the −21 residue of the leader sequence of HLA-B alleles, associated with low HLA-E surface expression and, consequently, higher expression of NKG2A[14]. Combined, these observations support that NK cells, in particular through the NKG2A axis, play a key role in post-treatment control of infection.

On the other hand, the higher frequency of NKp46^{-}NKp30^{-} NK cells may reflect a less inflamed environment. NKp30 and NKp46 are activating receptors expressed by NK cells that promote cytotoxicity upon engagement with self or pathogen-induced ligands[33], and their expression is enhanced by pro-inflammatory cytokines such as IL-12, IL-15 and IL-18[34] or type-I interferons. This may explain the distinct trajectories of NKG2A^{high}NKp30^{-}NKp46^{-} and NKG2A^{low}NKp30^{+}NKp46^{+} NK cells, with the former declining in blood, pLN and BM upon infection, whereas the latter accumulated in all these compartments during acute infection. In this context, the early initiation of ART may have contributed to preserve the NKG2A^{high}NKp30^{-} NKp46^{-} NK cell subset. A partial recovery of this population was observed in the tissues, particularly in pLN, but not in blood, after two years of ART, and their frequency in lymphoid tissues prior to ATI inversely correlated with the size of the SIV reservoir in pLN/mLN. This may reflect the capacity of the cells to traffic to infected tissues. Although NKG2A^{low} and NKG2A^{high} cells did not differ significantly in their expression of chemokine receptors, we observed a negative correlation between the homing potential of NKG2A^{high} cells and viremia during ATI, suggesting that tissue localization is critical. Notably, specific subsets of NKG2A^{high} cells expressed CXCR5 and CCR7, consistent with the potential to infiltrate lymph nodes and B follicles.

We also found profound differences in the effector capacities of NKG2A^{low} and NKG2A^{high} NK cells. NKG2A^{low} NK cells possessed a broad cytotoxic arsenal, carrying higher levels of both soluble (Granzyme B, Granzyme K, Perforin) and membrane-bound (FasL) cytolytic molecules. However, the NKG2A^{low}NKp30^{+}NKp46^{+} subset displayed significantly lower levels of Perforin and Granzyme at baseline compared to the broader NKG2A^{low} compartment, and these levels were further reduced upon infection. NKG2A^{low}NKp30^{+}NKp46^{+} cells also showed limited responsiveness to target cells and produced IL-17A and IL-10 in a bystander manner. By contrast, NKG2A^{high} NK cells were characterized by the production of antiviral cytokines (TNF-α, CCL4) and exhibited stronger degranulation upon stimulation with target cells. NKG2A^{high}NKp30^{-}

492 NKp46^{-} NK cells shared a similar functional profile with the other NKG2A^{high} NK cells,
493 suggesting that the former is the reflection of a particular immunological setting, and their
494 function was not affected by SIV infection. The cytokine-producing profile of these cells is
495 consistent with the NK cells residing in secondary lymphoid tissues in healthy and SIV-infected
496 macaques, rather than the highly cytotoxic subsets typically found in blood and mucosal tissues[35].
497 Therefore, NKG2A^{low}NKp30^{+}NKp46^{+} NK cells represent a functionality limited NK cell subset
498 that is further negatively impacted by infection, reflecting the impaired NK cell response
499 previously reported in HIV/SIV infections[36–38]. In contrast, NKG2A^{high}NKp30^{-}NKp46^{-} cells
500 represent a subset in which functional integrity is preserved despite infection.

501

502 Several studies have shown that NKG2A+ cells possess an enhanced capacity to respond to
503 autologous HIV-infected CD4+ T cells[39], particularly in the case of -21T homozygous
504 individuals[40], and that elite controllers carry particularly high frequencies of NKG2A^{+} NK
505 cells[37,41]. Moreover, in African green monkeys, natural hosts of SIV, NK cell responses within
506 lymph nodes are mediated through the MHC-E/NKG2A axis[24]. Therefore, it is possible that
507 NKG2A^{high} cells can migrate to lymph and recognize HIV- or SIV-infected cells through MHC-E
508 dependent (via antigen presentation[42,43] or the "missing-self" axis upon MHC-E
509 downregulation)[44] or independent mechanisms, leading to the production of antiviral soluble
510 molecules such as TNF-α and CCL4[19]. In addition to a direct antiviral role, NK cells may
511 contribute to the orchestration of other immune responses. We previously reported that SIV PTC
512 from the pVISCONTI study were characterized by the presence of enhanced CD8 T-cells with
513 memory traits in secondary lymph nodes, capable of exerting a superior antiviral pressure to
514 counteract viral rebound after ATI[25]. β-chemokines produced by NK cells could promote the
515 recruitment of T-cells to the site of infection[45]. Moreover, reduced expression of NKp30, and at a
516 lesser extent NKp46, may protect dendritic cells from NK cell-mediated killing[46], thereby
517 favoring the priming of such CD8+ T cells. In contrast, IL-10 producing-

518 NKG2A^{low}NKp30^{+}NKp46^{+} NK cells may contribute to dendritic cell depletion[47], CD8+ T cell
519 dysfunction and to the establishment and persistence of the SIV reservoir[48].

520

521 Overall, these findings suggest that a superior MHC-driven NKG2A^{high} vs NKG2A^{low} balance,
522 coupled with low baseline inflammation, sets a favorable stage for an improved response against
523 SIV/HIV during ART interruption. They further indicate that the early preservation of specific
524 NK cell subsets through therapeutic intervention may be critical for controlling viral rebound
525 following ATI. Together, these results underscore the pivotal role of the NKG2A pathway in
526 shaping NK cell responses during infection and treatment and highlight the potential of harnessing
527 this axis in novel therapeutic strategies aimed at achieving durable HIV remission.

528

Acknowledgments

The authors thank Animalliance and animal care workers for expert technical assistance at IDMIT. The authors also thank the Cytometry and the Biomarkers UTechS platforms at Institut Pasteur and the members of the ANRS RHIVIERA and ERASE HIV consortia for helpful discussions, FTC, DTG, and TDF were obtained from Gilead and ViiV Healthcare through the "IAS Toward an HIV Cure" common Material Transfer Agreement. The pVISCONTI study was funded by MSDAVENIR through a research grant to the ANRS RHIVIERA consortium. This work was also supported by UM1AI16456, co-funded by NIH/NHLBI/NIDDK/NINDS/NIDA/NIAID and by the NIAID. LRM received support from the EU under the Marie Sklodowska-Curie action program and AC was supported by an ANRS-MIE Postdoctoral Fellowship. The funders had no role in study design, data collection and analysis, decision to publish or preparation of the manuscript.

Author contributions

LRM, AC and CP designed the experiments. LRM, AC, CP, VM, AM, ND, AD performed experiments and analyzed data. VAF, RLG and AS-C analyzed data. DD, NDB, CR, MM-T contributed to conception, study design and analyzed/discussed the data. RLG and AS-C conceived the study and provided financial support. AS-C supervised the study. LRM and AS-C wrote the original draft. All the authors reviewed and edited the final manuscript.

References

1. Fidler, S. *et al.* Virological blips and predictors of post treatment viral control after stopping ART started in primary HIV infection. *J. Acquir. Immune Defic. Syndr.* **74**, 126–133 (2017).

2. Sáez-Cirión, A. *et al.* Post-Treatment HIV-1 Controllers with a Long-Term Virological Remission after the Interruption of Early Initiated Antiretroviral Therapy ANRS VISCONTI Study. *PLOS Pathog.* **9**, e1003211 (2013).

3. Chéret, A. *et al.* Combined ART started during acute HIV infection protects central memory CD41 T cells and can induce remission. *J. Antimicrob. Chemother.* **70**, 2108–2120 (2015).

4. Hocqueloux, L. *et al.* Long-term antiretroviral therapy initiated during primary HIV-1 infection is key to achieving both low HIV reservoirs and normal T cell counts. *J. Antimicrob. Chemother.* **68**, 1169–1178 (2013).

5. Namazi, G. *et al.* The control of HIV after antiretroviral medication pause (CHAMP) study: Posttreatment controllers identified from 14 clinical studies. *J. Infect. Dis.* **218**, 1954–1963 (2018).

6. Gunst, J. D. *et al.* Time to HIV viral rebound and frequency of post-treatment control after analytical interruption of antiretroviral therapy: an individual data-based meta-analysis of 24 prospective studies. *Nat. Commun.* **16**, 906 (2025).

7. Massanella, M. *et al.* Long-term effects of early antiretroviral initiation on HIV reservoir markers: a longitudinal analysis of the MERLIN clinical study. *The Lancet Microbe* **2**, e198–e209 (2021).

8. Schuetz, A. *et al.* Initiation of ART during Early Acute HIV Infection Preserves Mucosal Th17 Function and Reverses HIV-Related Immune Activation. *PLoS Pathog.* **10**,

e1004543 (2014).

9. Takata, H. *et al.* Long-term antiretroviral therapy initiated in acute HIV infection prevents residual dysfunction of HIV-specific CD8+ T cells. *eBioMedicine* **84**, 104253 (2022).

10. Assoumou, L. *et al.* A low HIV-DNA level in peripheral blood mononuclear cells at antiretroviral treatment interruption predicts a higher probability of maintaining viral control. *AIDS* **29**, 2003–2007 (2015).

11. Sharaf, R. *et al.* HIV-1 proviral landscapes distinguish posttreatment controllers from noncontrollers. *J. Clin. Invest.* **128**, 4074–4085 (2018).

12. Trémeaux, P. *et al.* In-Depth Characterization of Full-Length Archived Viral Genomes after Nine Years of Posttreatment HIV Control. *Microbiol. Spectr.* **11**, e0326722 (2023).

13. Essat, A. *et al.* A genetic fingerprint associated with durable HIV remission after interruption of antiretroviral treatment: ANRS VISCONTI/PRIMO. *Med* **6**, 100670 (2025).

14. Horowitz, A. *et al.* Class I HLA haplotypes form two schools that educate NK cells in different ways. *Sci. Immunol.* **1**, eaag1672 (2016).

15. Etemad, B. *et al.* HIV post-treatment controllers have distinct immunological and virological features. *Proc. Natl. Acad. Sci. U. S. A.* **120**, e2218960120 (2023).

16. Climent, N. *et al.* Immunological and virological findings in a patient with exceptional post-treatment control: a case report. *Lancet HIV* **10**, e42–e51 (2023).

17. Madhavi, V. *et al.* HIV-1 Env- and Vpu-Specific Antibody-Dependent Cellular Cytotoxicity Responses Associated with Elite Control of HIV. *J. Virol.* **91**, e00700-17 (2017).

18. Haynes, B. F. *et al.* Immune-Correlates Analysis of an HIV-1 Vaccine Efficacy Trial. *N. Engl. J. Med.* **366**, 1275–86 (2012).

19. Fehniger, T. A. *et al.* Natural Killer Cells from HIV-1+ Patients Produce C-C Chemokines and Inhibit HIV-1 Infection. *J. Immunol.* **161**, 6433–8 (1998).

20. Morandi, B., Bougras, G., Muller, W. A., Ferlazzo, G. & Münz, C. NK cells of human secondary lymphoid tissues enhance T cell polarization via IFN-γ secretion. *Eur. J. Immunol.* **36**, 2394–400 (2006).

21. Lee, S. H., Kim, K. S., Fodil-Cornu, N., Vidal, S. M. & Biron, C. A. Activating receptors promote NK cell expansion for maintenance, IL-10 production, and CD8 T cell regulation during viral infection. *J. Exp. Med.* **206**, 2235–2251 (2009).

22. Kilian, M. *et al.* The immunoglobulin superfamily ligand B7H6 subjects T cell responses to NK cell surveillance. *Sci. Immunol.* **9**, eadj7970 (2024).

23. Rascle, P. *et al.* NK cell spatial dynamics and IgA responses in gut-associated lymphoid tissues during SIV infections. *Commun. Biol.* **5**, 674 (2022).

24. Huot, N. *et al.* SIV-induced terminally differentiated adaptive NK cells in lymph nodes associated with enhanced MHC-E restricted activity. *Nat. Commun.* **12**, 1282 (2021).

25. Passaes, C. *et al.* Early antiretroviral therapy favors post-treatment SIV control associated with the expansion of enhanced memory CD8+ T-cells. *Nat. Commun.* **15**, 178 (2024).

26. Neildez, O. *et al.* Selective quasispecies transmission after systemic or mucosal exposure of macaques to simian immunodeficiency virus. *Virology* **243**, 12–20 (1998).

27. Hofmann-Lehmann, R. *et al.* Sensitive and robust one-tube real-time reverse transcriptase-polymerase chain reaction to quantify SIV RNA load: Comparison of one- versus two-enzyme systems. *AIDS Res. Hum. Retroviruses* **16**, (2000).

28. Morán-Plata, F. J. *et al.* A novel NKp80-based strategy for universal identification of normal, reactive and tumor/clonal natural killer-cells in blood. *Front. Immunol.* **15**, 1423689 (2024).

29. Orrantia, A. *et al.* A NKp80-Based Identification Strategy Reveals that CD56neg NK Cells Are Not Completely Dysfunctional in Health and Disease. *iScience* **23**, 101298 (2020).

30. Mavilio, D. *et al.* Characterization of $CD56^{-}/CD16^{+}$ natural killer (NK) cells: A highly dysfunctional NK subset expanded in HIV-infected viremic individuals. *Proc. Natl. Acad. Sci.* **102**, 2886–2891 (2005).

31. Mee, E. T. *et al.* Mhc haplotype H6 is associated with sustained control of SIVmac251 infection in Mauritian cynomolgus macaques. *Immunogenetics* **61**, 327–339 (2009).

32. Wiseman, R. W. *et al.* Simian Immunodeficiency Virus SIVmac239 Infection of Major Histocompatibility Complex-Identical Cynomolgus Macaques from Mauritius. *J. Virol.* **81**, 349–361 (2007).

33. Hadad, U. *et al.* NKp46 clusters at the immune synapse and regulates NK cell polarization. *Front. Immunol.* **6**, 495 (2015).

34. Boieri, M. *et al.* IL-12, IL-15, and IL-18 pre-activated NK cells target resistant T cell acute lymphoblastic leukemia and delay leukemia development in vivo. *Oncoimmunology* **6**, e1274478 (2017).

35. Huot, N. *et al.* Non-human Primate Determinants of Natural Killer Cells in Tissues at Steady-State and During Simian Immunodeficiency Virus Infection. *Front. Immunol.* **11**, 2134 (2020).

36. LaBonte, M. L., McKay, P. F. & Letvin, N. L. Evidence of NK cell dysfunction in SIV-infected rhesus monkeys: Impairment of cytokine secretion and NKG2C/C2 expression. *Eur. J. Immunol.* **36**, 2424–33 (2006).

37. Romero-Martín, L. *et al.* Disruption of the HLA-E/NKG2X axis is associated with uncontrolled HIV infections. *Front. Immunol.* **13**, 1027855 (2022).

38. Alter, G. *et al.* Sequential deregulation of NK cell subset distribution and function

starting in acute HIV-1 infection. *Blood* **106**, 3366–9 (2005).

39. Lisovsky, I. *et al.* A Higher Frequency of NKG2A + than of NKG2A − NK Cells Responds to Autologous HIV-Infected CD4 Cells irrespective of Whether or Not They Coexpress KIR3DL1 . *J. Virol.* **89**, 9909–19 (2015).

40. Merino, A. M. *et al.* Dimorphic HLA-B signal peptides differentially influence HLA-E- and natural killer cell-mediated cytolysis of HIV-1-infected target cells. *Clin. Exp. Immunol.* **174**, 414–423 (2013).

41. Sánchez-Gaona, N. *et al.* NKG2C and NKG2A coexpression defines a highly functional antiviral NK population in spontaneous HIV control. *JCI Insight* **9**, e182660 (2024).

42. Jost, S. *et al.* Antigen-specific memory NK cell responses against HIV and influenza use the NKG2/HLA-E axis. *Sci. Immunol.* **8**, eadi3974 (2023).

43. Davis, Z. B. *et al.* A Conserved HIV-1-Derived Peptide Presented by HLA-E Renders Infected T-cells Highly Susceptible to Attack by NKG2A/CD94-Bearing Natural Killer Cells. *PLoS Pathog.* **12**, e1005421 (2016).

44. van Stigt Thans, T. *et al.* Primary HIV-1 Strains Use Nef To Downmodulate HLA-E Surface Expression. *J. Virol.* e00719-19 (2019).

45. Niño, J. L. G. *et al.* Cytotoxic T cells swarm by homotypic chemokine signalling. *Elife* **9**, e56554 (2020).

46. Castriconi, R. *et al.* Transforming growth factor β1 inhibits expression of NKp30 and NKG2D receptors: Consequences for the NK-mediated killing of dendritic cells. *Proc. Natl. Acad. Sci.* **100**, 4120–4125 (2003).

47. Alter, G. *et al.* IL-10 induces aberrant deletion of dendritic cells by natural killer cells in the context of HIV infection. *J. Clin. Invest.* **120**, 1905–1913 (2010).

48. Harper, J. *et al.* Interleukin-10 contributes to reservoir establishment and persistence in SIV-infected macaques treated with antiretroviral therapy. *J. Clin. Invest.* **132**, e155251

(2022).

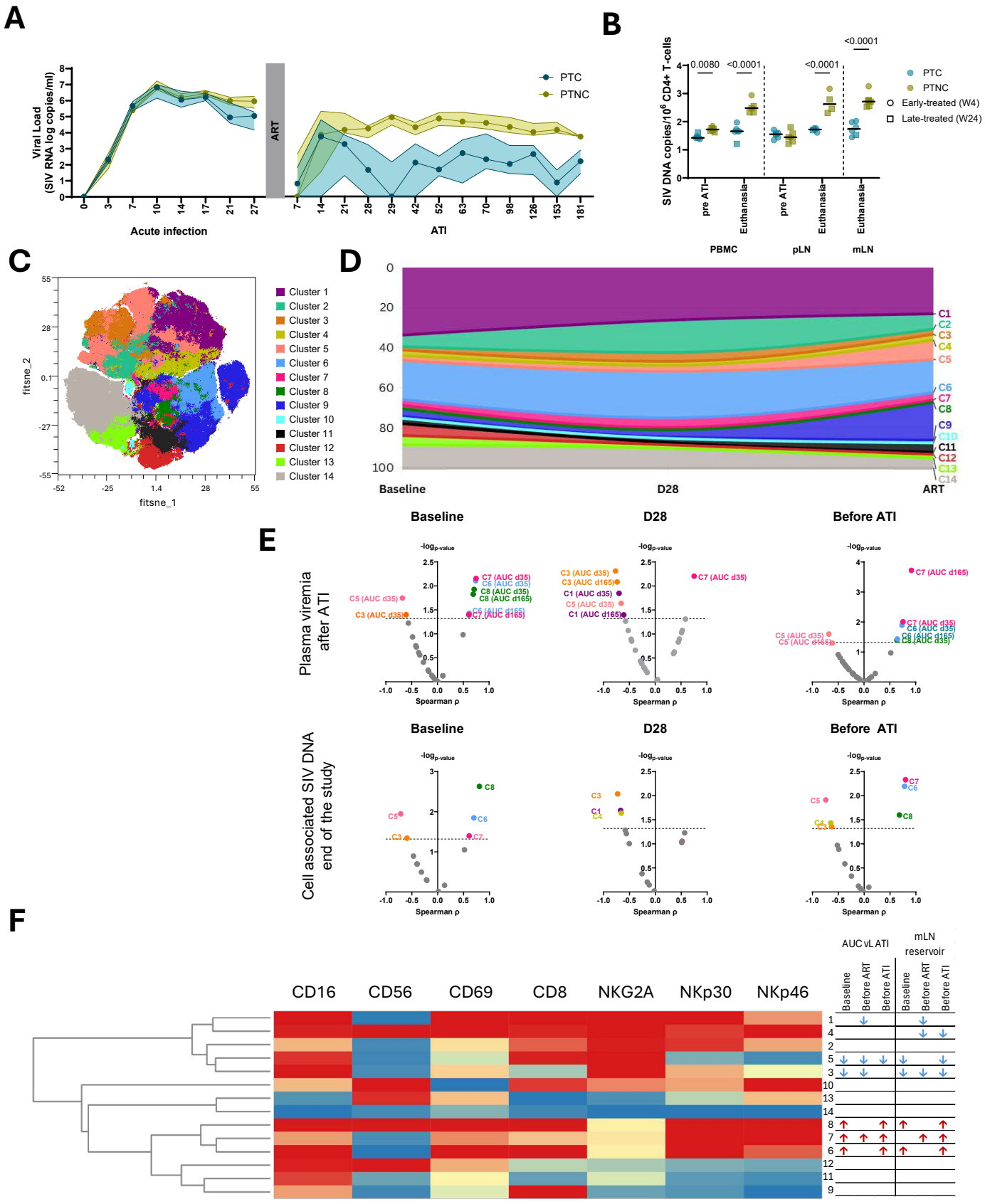


Figure 1. Unsupervised analysis of NK cell dynamics during the pVISCONTI study. (A) Viral load (SIV RNA copies/mL) during the study. (**B**) Viral reservoir (SIV DNA copies/10^6 CD4+ T-cells). (**C**) Dimensional reduction and unsupervised on CD3-CD14-CD20-NKp80+ cells identified 14 different clusters of NK cells based on the expression of CD16, CD56, CD69, CD8, NKG2A, NKp30, NKp46. (**D**) Relative abundance of the 14 clusters in PBMC at the Baseline, before ART and before ATI. (**E**) Volcano plots showing p-value and Spearman ρ of the correlation between cluster abundance and AUC of viral load during ATI (top) or total SIV DNA copies/10^6 $CD4^+$ T-cells in mesenteric lymph nodes (mLN) at euthanasia (bottom). (**F**) Relative expression of the different markers that defined the 14 clusters. Dimensional reduction was performed by Fit-tSNE and clustering by FlowSOM. Multiple comparison was performed by Two-way ANOVA and False Discovery Rate (FDR) correction. Correlations were performed by Spearman-Pearson. Significant values were considered when p-value<0.05 and q-value<0.05.

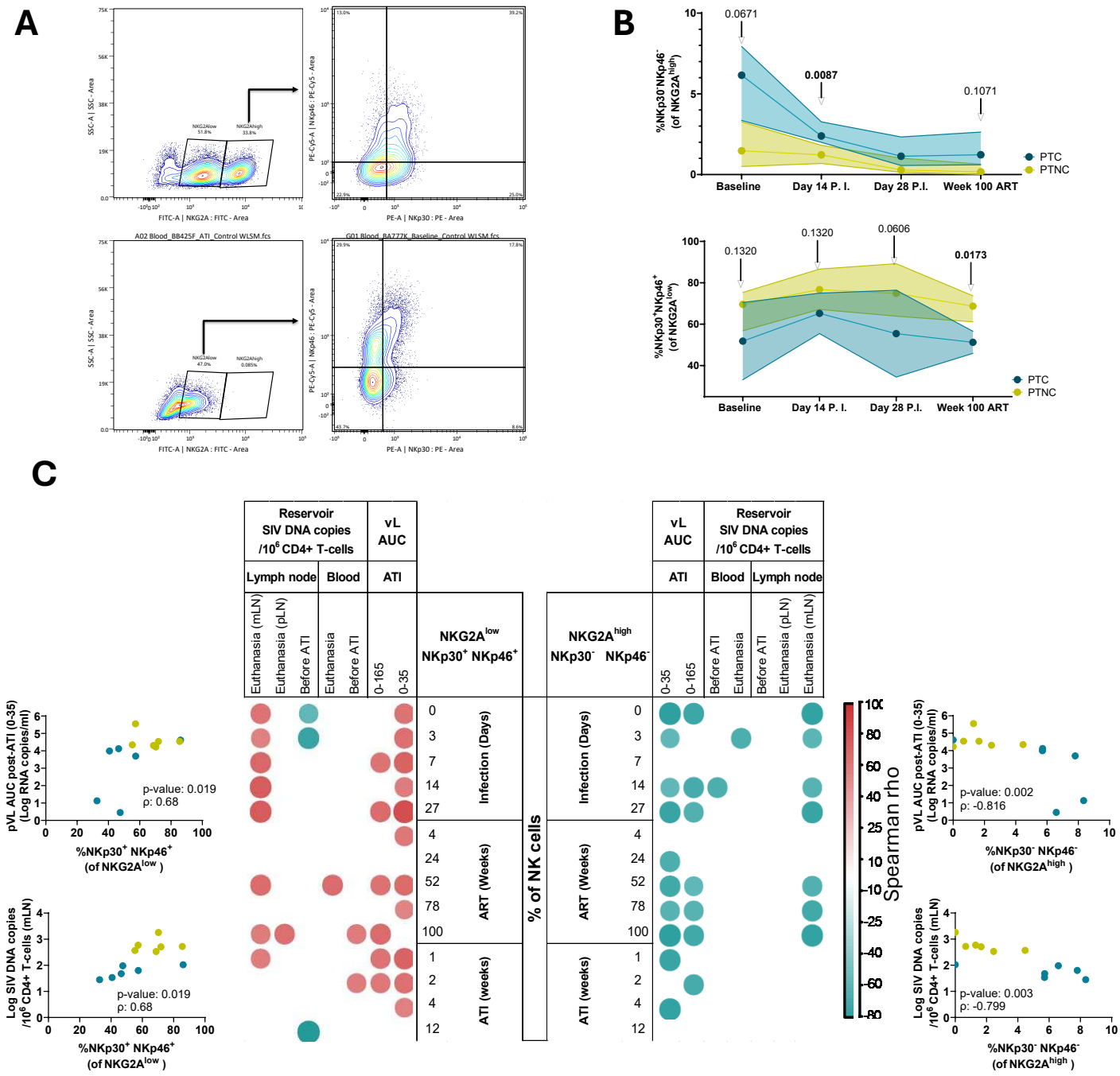
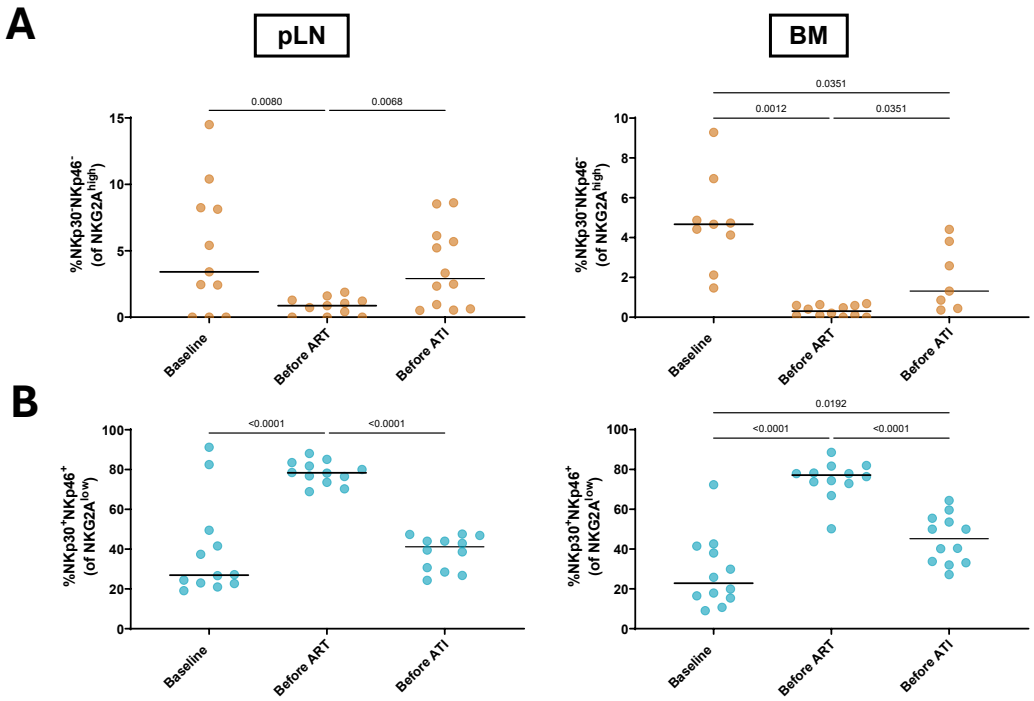


Figure 2. NKG2A^{high}NKp30^{-}NKp46^{-} and NKG2A^{low}NKp30^{+}NKp46^{+} dynamic. (**A**) Gating strategy for NKG2A^{high}NKp30^{-}NKp46^{-} (top) and NKG2A^{low}NKp30^{+}NKp46^{+} (bottom) cells. (**B**) Frequency of NKG2A^{high}NKp30^{-}NKp46^{-} (top) or NKG2A^{low}NKp30^{+}NKp46^{+} (bottom) cells during acute infection and before ATI in PTC (turquoise) and PTNC (green). **(C)** Correlations of baseline frequency of NKG2A^{low}NKp30^{+}NKp46^{+} cells and AUC of viral load during ATI and SIV reservoir in the mesenteric lymph node at Euthanasia (left). Correlogram showing the positive (red) and negative (blue) correlations between NKG2A^{high}NKp30^{-}NKp46^{-} cells (left) and NKG2A^{low}NKp30^{+}NKp46^{+} cells (right) with the AUC of viral load during ATI and total SIV DNA copies/10^{6} CD4^{+} T-cells (center). Correlations of baseline frequency of NKG2A^{high}NKp30^{-}NKp46^{-} cells and AUC of viral load during ATI and SIV reservoir in the mesenteric lymph node at Euthanasia (right). Group comparisons were performed by Mann-Whitney test. Correlations were performed by Spearman-Pearson. Significant values were considered when p-value<0.05 and q-value<0.05. Only significant correlations are depicted in the correlogram.



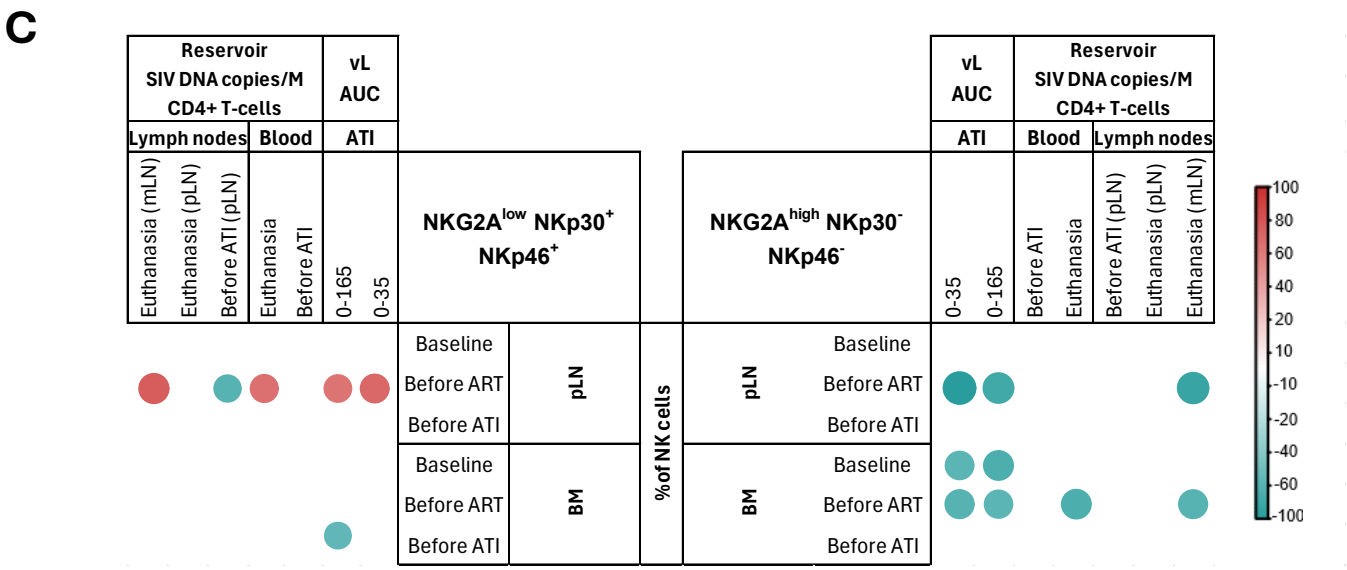


Figure 3. NKG2A^{high}NKp30^{-}NKp46^{-} and NKG2A^{low}NKp30^{+}NKp46^{+} dynamic in tissues. (A) Frequency of NKG2A^{high}NKp30^{-}NKp46^{-} cells in the pLN and BM at the baseline, before ART and before ATI. (**B**) Frequency of NKG2A^{low}NKp30^{+}NKp46^{+} cells in the pLN and BM at the baseline, before ART and before ATI. (**C**) Correlogram showing the positive (red) and negative (cyan) correlations between NKG2A^{high}NKp30^{-}NKp46^{-} cells (right) and NKG2A^{low}NKp30^{+}NKp46^{+} cells (left) with the AUC of viral load during ATI and total SIV DNA copies/10^{6} CD4^{+} Multiple comparison was performed by Two-way ANOVA with False Discovery Rate (FDR) correction. Correlations were performed by Spearman-Pearson. Significant values were considered when p-value<0.05 and q-valu q-value<0.05. Only significant correlations are depicted in the correlogram.

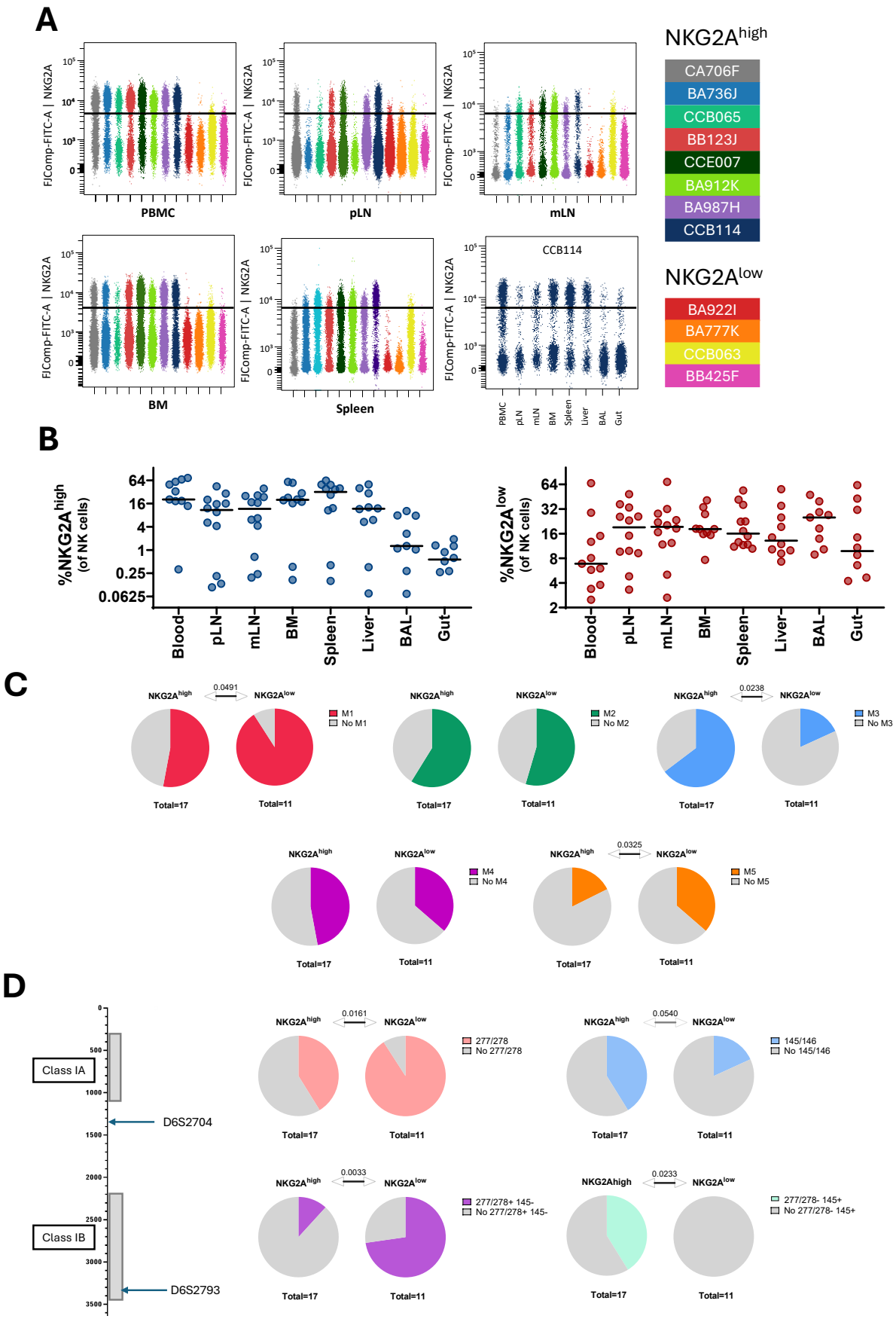


Figure 4. Physiological determinants of NKG2A^{high} expression. (**A**) The presence or absence of NKG2A^{high} NK cells is constitutive and observed across different lymphoid tissues. The last graph is representative of all tissues in one animal CCB114) (**B**) Frequency of NKG2A^{high} and NKG2A^{low} cells in different tissues. (**C**) Absolute frequency of macaques harboring or not NKG2A^{high} cells based on M1, M2, M3, M4 or M5 MHC haplotypes. (**D**) Localization and properties of the 277 and 145 microsatellite markers in the MHC region of cynomolgus macaques (adapted from *Wiseman et al.*). (**E**) Absolute frequency of macaques harboring or not NKG2A^{high} cells based on the 277 and/or 145 satellites.. Fisher's exact test test was applied to evaluate absolute frequencies. Significant values were considered when p-value<0.05.

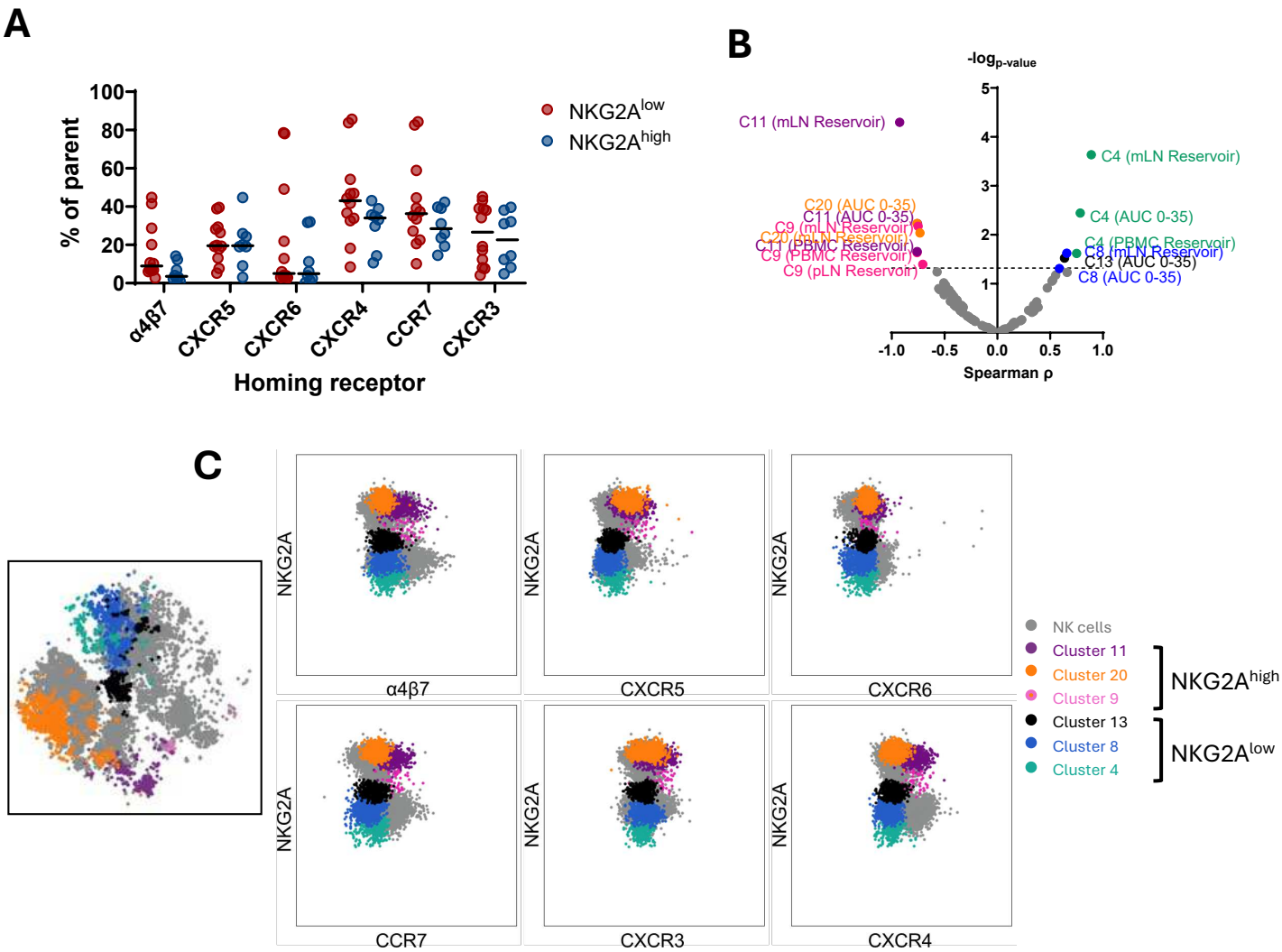
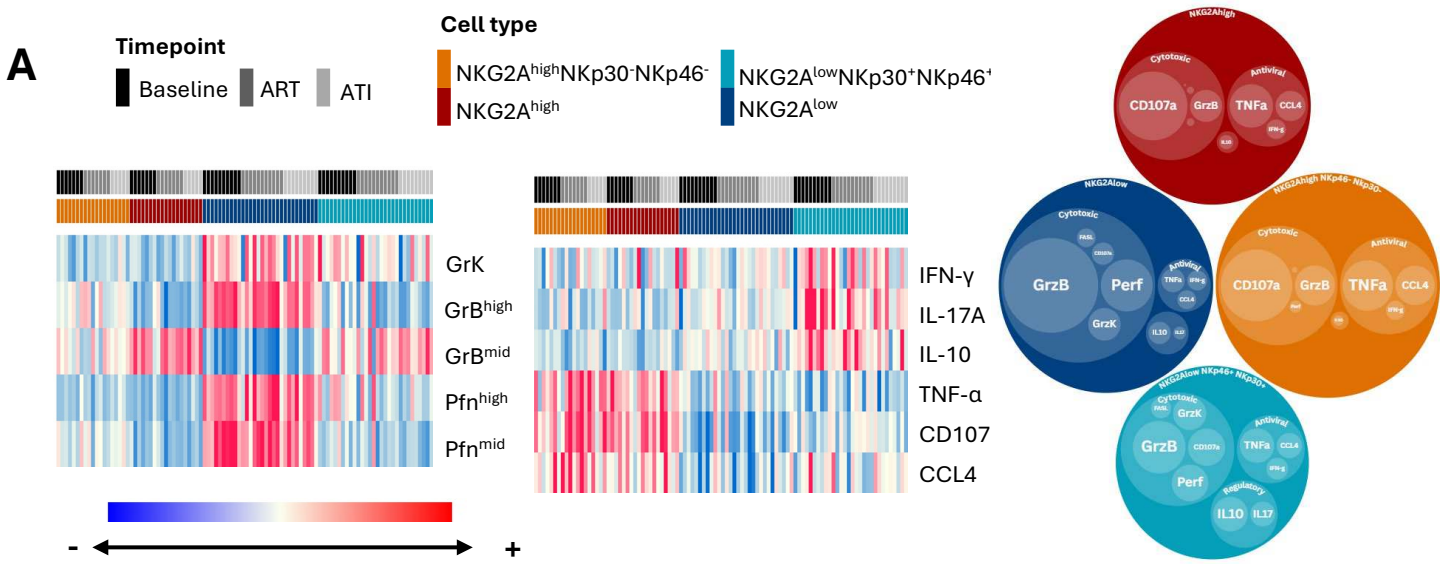
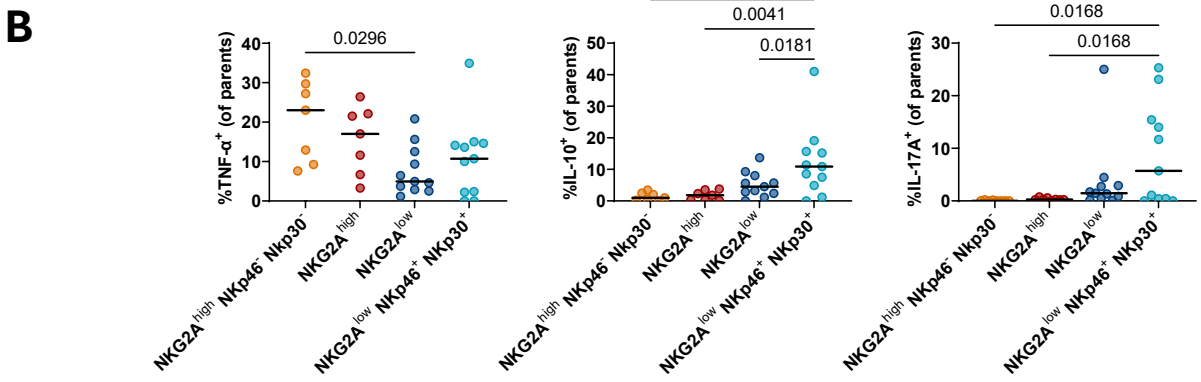
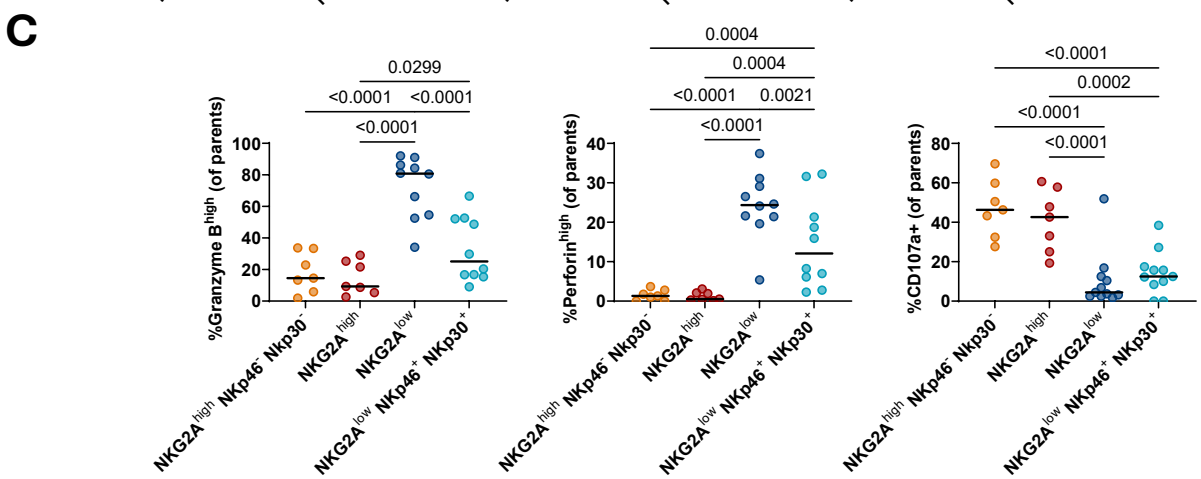


Figure 5. Expression of homing markers in NK cells before ATI. (A) Expression of homing markers in NKG2Alow (red) and NKG2A^{high} (blue) cells. Dimensional reduction and unsupervised on CD3-CD14-CD20-NKp80+ cells acquired before ATI identified 14 different clusters of NK cells based on the expression of NKG2A, Integrin α4β7, CXCR5, CXCR6, CCR7, CXCR3 and CXCR4 of which 6 (Clusters 4, 8, 9, 11, 13 and 20) showed positive or negative correlation with the AUC during ATI and/or total SIV DNA. **(B)** Volcano plots showing p-value and Spearman ρ of the correlation between cluster abundance in PBMC AUC of viral load during ATI and total SIV DNA copies/10^6 CD4$^+$ T-cell. **(C)** Expression of homing markers Integrin α4β7, CXCR5, CXCR6, CCR7, CXCR3 and CXCR4 in clusters 4, 8, 9, 11, 13 and 20. Multiple comparison was performed by Two-way ANOVA and False Discovery Rate (FDR) correction. Correlations were performed by Spearman-Pearson. Dimensional reduction was performed by Fit-tSNE and clustering by FlowSOM.







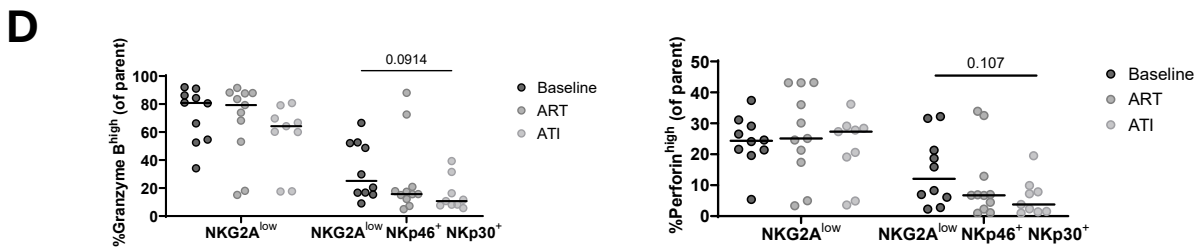


Figure 6. Functional properties of NKG2A^{high} (red), NKG2A^{high}NKp30^{-}NKp36^{-} (orange), NKG2A^{low} (navy blue) and NKG2A^{low}NKp30^{+}NKp46^{+} (turquoise). (**A**). Cytotoxic potential of unstimulated NK cells (left) and cytokine production in NK cells stimulated with target cells in an effector:target ratio = 2:1 for 4h (right). (**B**). Comparison of TNF-a (top, left), IL-10 (top, middle) and IL-17A (top, right) production in NKG2A^{high}, NKG2A^{high}NKp30^{-}NKp36, NKG2A^{low} and NKG2A^{low}NKp30^{+}NKp46^{+}. (**C**) Granzyme B^{high} (bottom, left) and Perforin^{high} (bottom, middle) and CD107a (bottom, right) production in NKG2A^{high}, NKG2A^{high}NKp30^{-}NKp36, NKG2A^{low} and NKG2A^{low}NKp30^{+}NKp46^{+}. (**D**) Comparison of Granzyme B^{high} (left) and Perforin^{high} (right) levels in NKG2A^{low} and NKG2A^{low}NKp30^{+}NKp46^{+} cells over time. Multiple comparisons were performe by Two-way ANOVA with FDR rate post-hoc correction. Significant values were considered when p-value<0.05 and q-value<0.05.

Table S1. Characteristics of Cynomolgus macaques included in the study

							Cumulated Viremia post-ATI (copies/mL)		Cell associated SIV DNA- End of study (copies/10^6 cells)		
ID	Age (years)	Weight (kg)	Haplotype	NKG2A	ART initiation	Outcome after ATI	0-35 days	0-165 days	PBMC	pLN	mLN
BA777K	4.8	6.7	M2/M1	low	W4	PTNC	16 770	343 612	871	1 479	1 820
BA9221	5.8	5.4	M1/M3	low	W4	PTC	41 312	44 620	93	41	105
BB425F	5.1	5.8	M1/M2M5	low	W24	PTNC	357 190	619 709	214	NA	589
CCB063	4.2	6.1	M1/M2M5	low	W24	PTNC	34 701	67 463	302	617	525
CA706F	4.1	4.4	M5/M4M1M2	high	W4	PTC	13 329	17 488	46	52	48
BA736J	5.2	5.5	M1M2M1/M4	high	W4	PTC	3	4 323	46	NA	95
CCB065	4.2	6.4	M3/M4	high	W4	PTC	13	38	54	58	28
BB123J	5.2	5.8	M2M1/M3	high	W4	PTC	4 979	8 724	45	58	63
BA912K	4.8	5	M1/M2	high	W24	PTNC	34 470	448 404	NA	NA	513
BA987H	5.1	5.8	M4/M3	high	W24	PTC	9 868	11 312	16	50	34
CCB114	4.2	4.6	M3M4/M2	high	W24	PTNC	22 149	123 825	355	204	372
CCE007	4	4.7	M1/M3	high	W24	PTNC	20 267	116 167	214	288	339

Analytical treatment interruption, ATI; Post-treatment controller, PTC; post-treatment non controller, PTNC; not-available, NA; peripheral lymph nodes, pLN; mesenteric lymph nodes, mLN

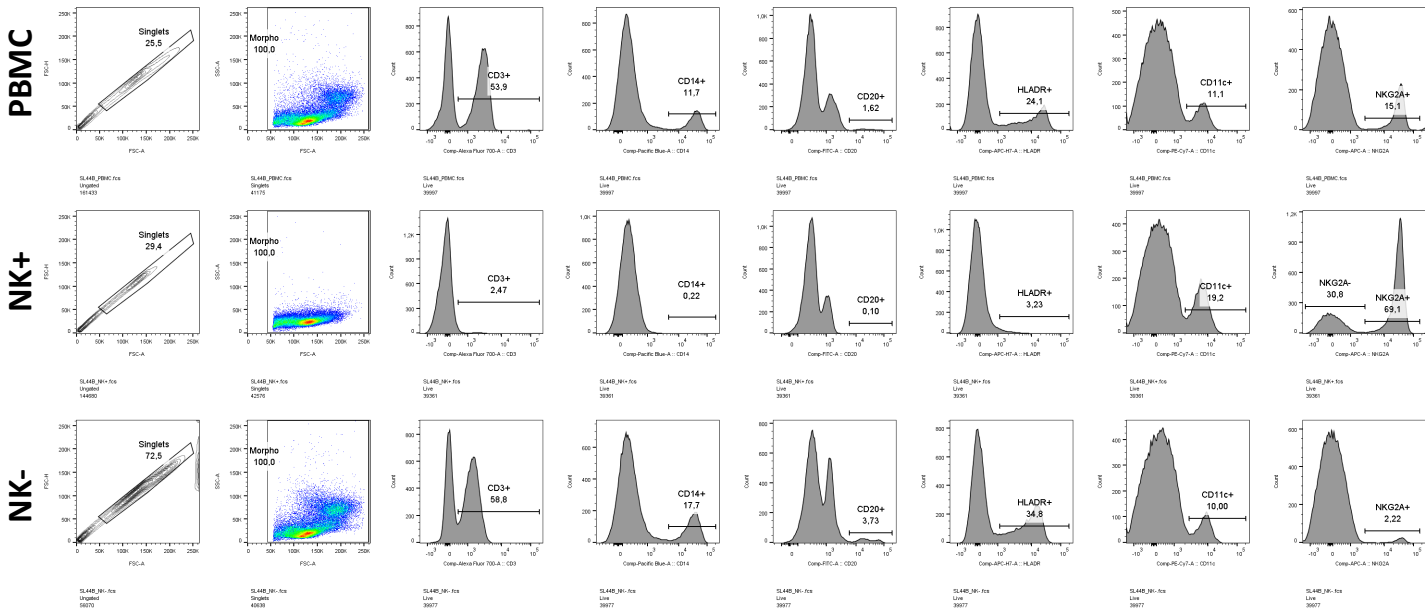


Figure S1. Efficiency of the custom NHP NK isolation kit (Miltenyi).

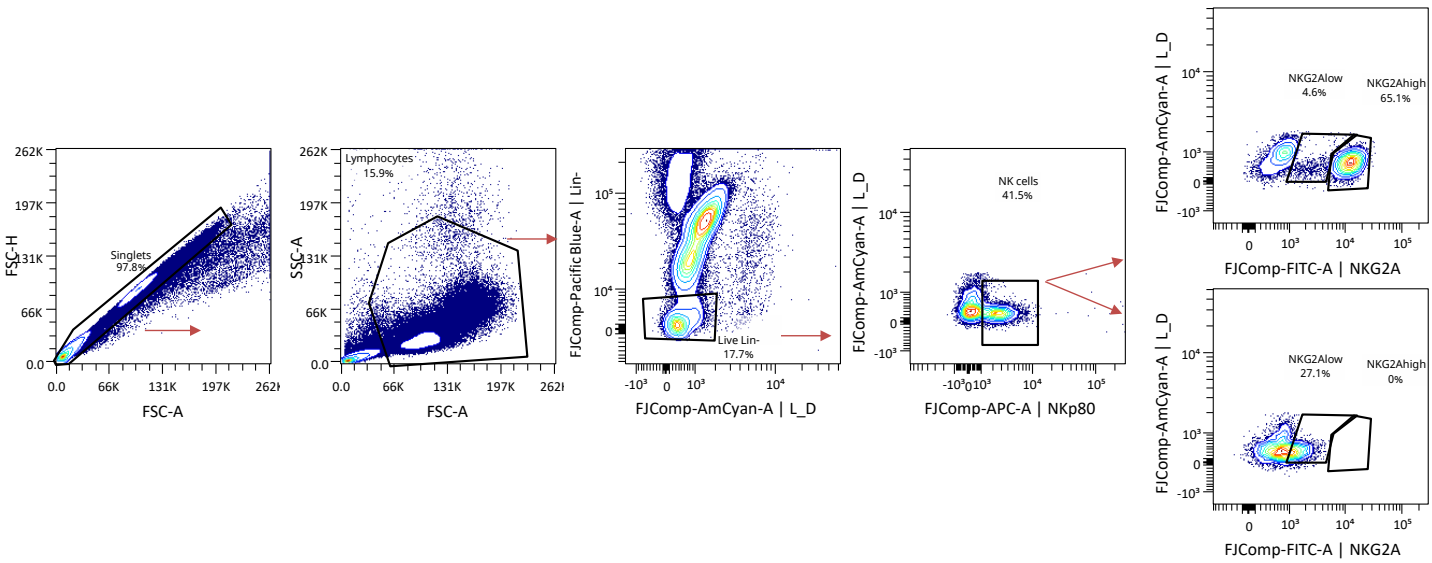


Figure S2. Gating strategy for NKG2A^{high} cells (right, top) and NKG2A^{low} (right, bottom) on NKp80^{+} cells.

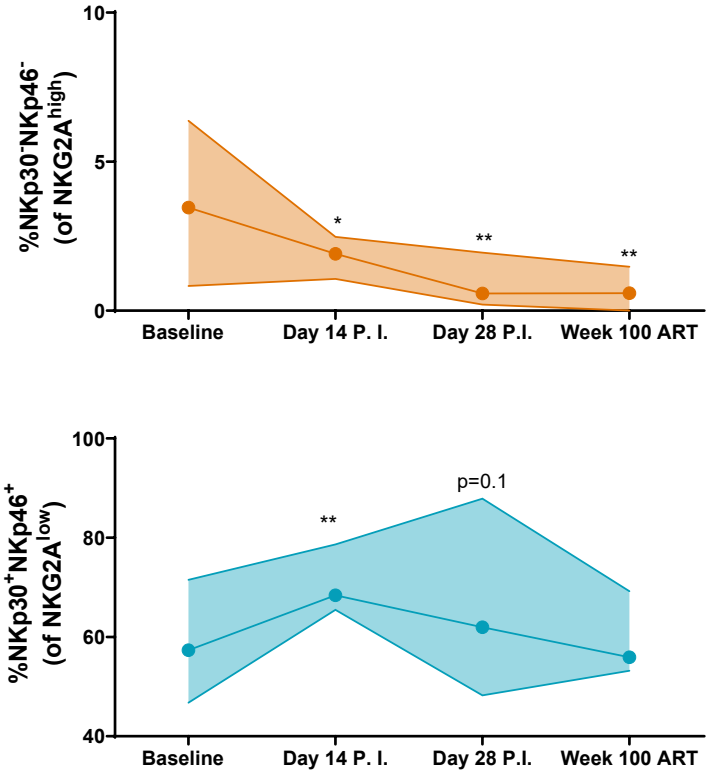


Figure S3. NKG2A^{high}NKp30^{-}NKp46^{-} and NKG2A^{low}NKp30^{+}NKp46^{+} dynamics in macaques. Frequency of NKG2A^{high}NKp30^{-}NKp46^{-} (top) or NKG2A^{low}NKp30^{+}NKp46^{+} (bottom) cells at the baseline, during acute infection and before ATI.

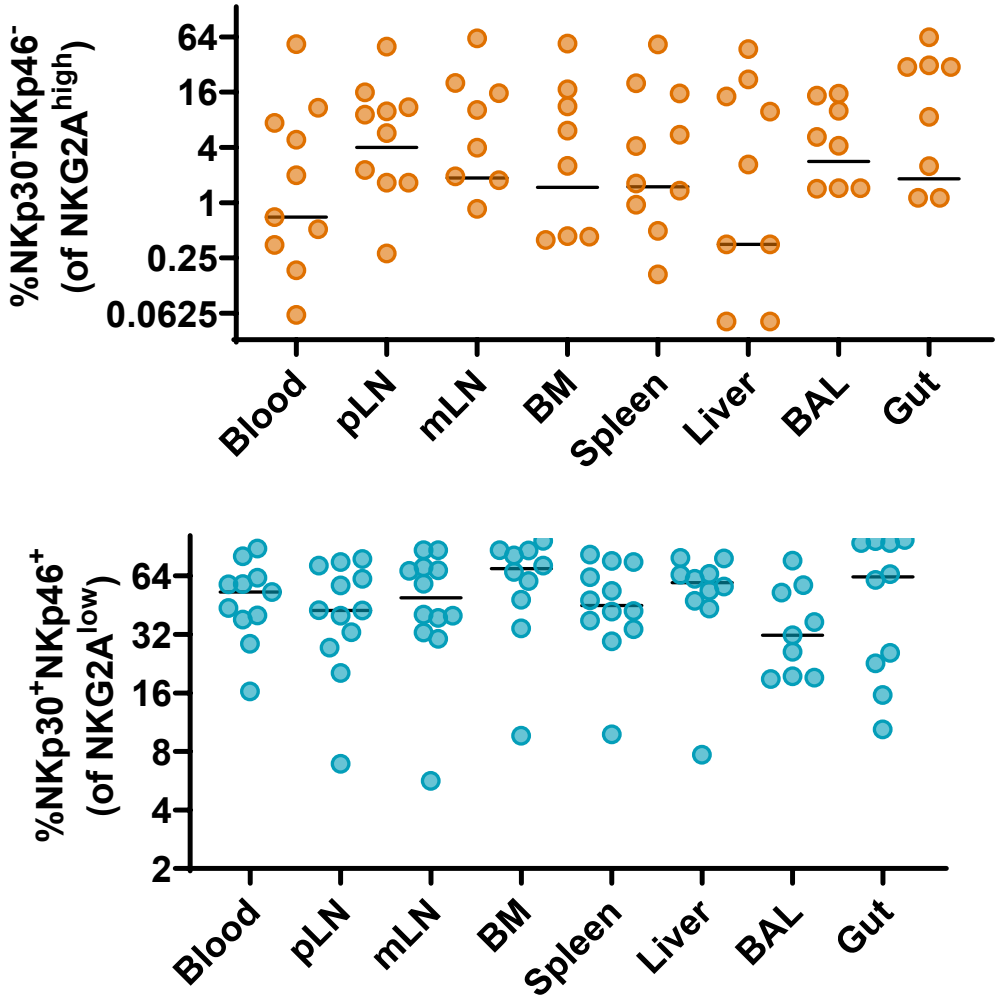


Figure S4. Abundance of NKG2A^{high}NKp30^{-}NKp46^{-} (top, orange) and NKG2A^{low}NKp30^{+}NKp46^{+} (bottom) in different tissues at euthanasia (bottom, blue).

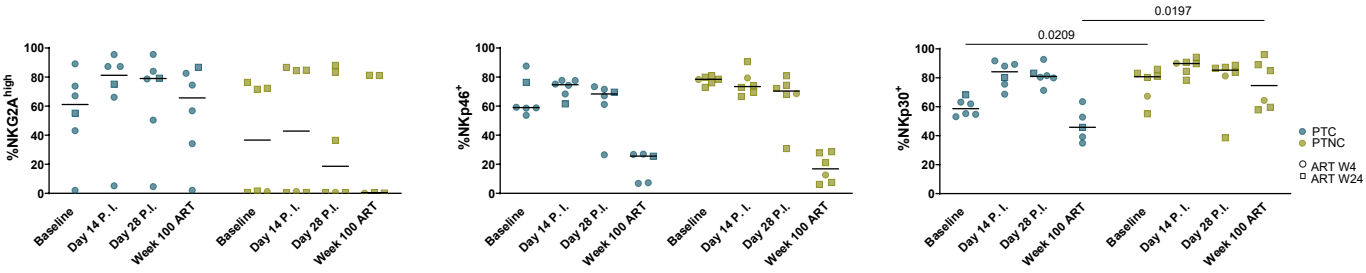


Figure S5. Frequency of NKG2A^{high} (left), NKp46^{+} (middle) and NKp30^{+} (right) cells during the study in PTC (blue) and PTNC (green) at the baseline, during acute infection and before ATI.

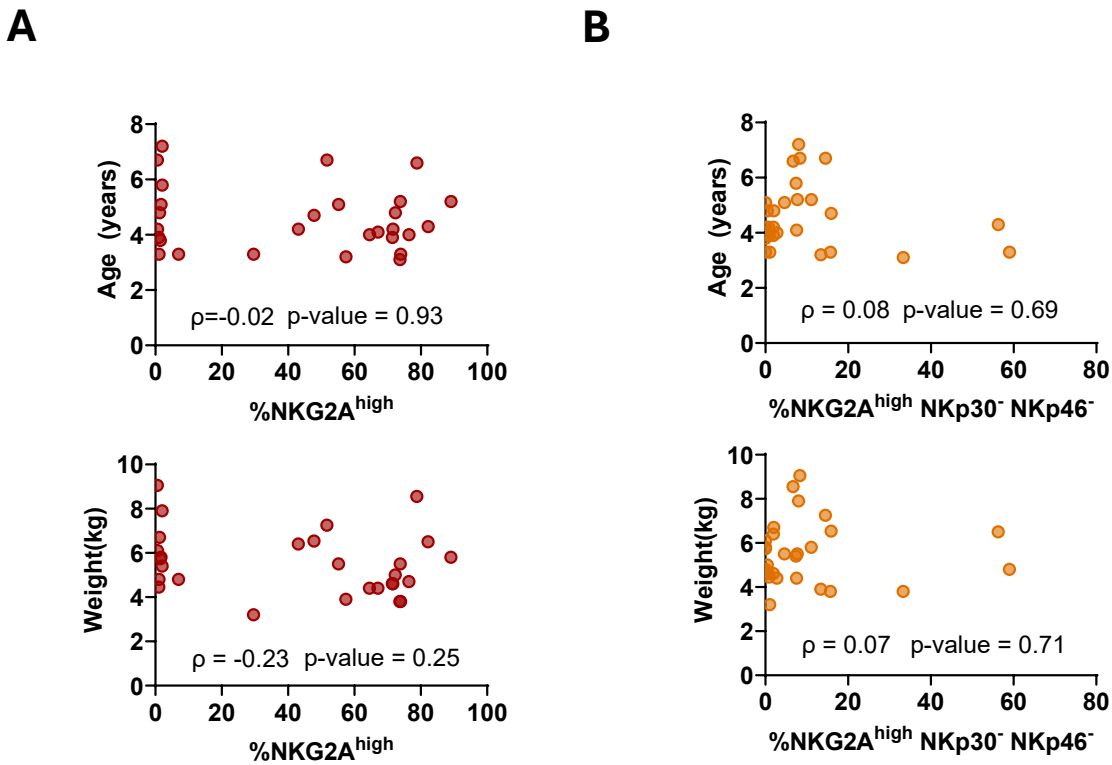


Figure S6. Correlation between the frequency of NKG2A^{high} cells (left) and NKG2A^{high}NKp30^{-} NKp46^{-} (right) at the baseline with age and weight (n=28).

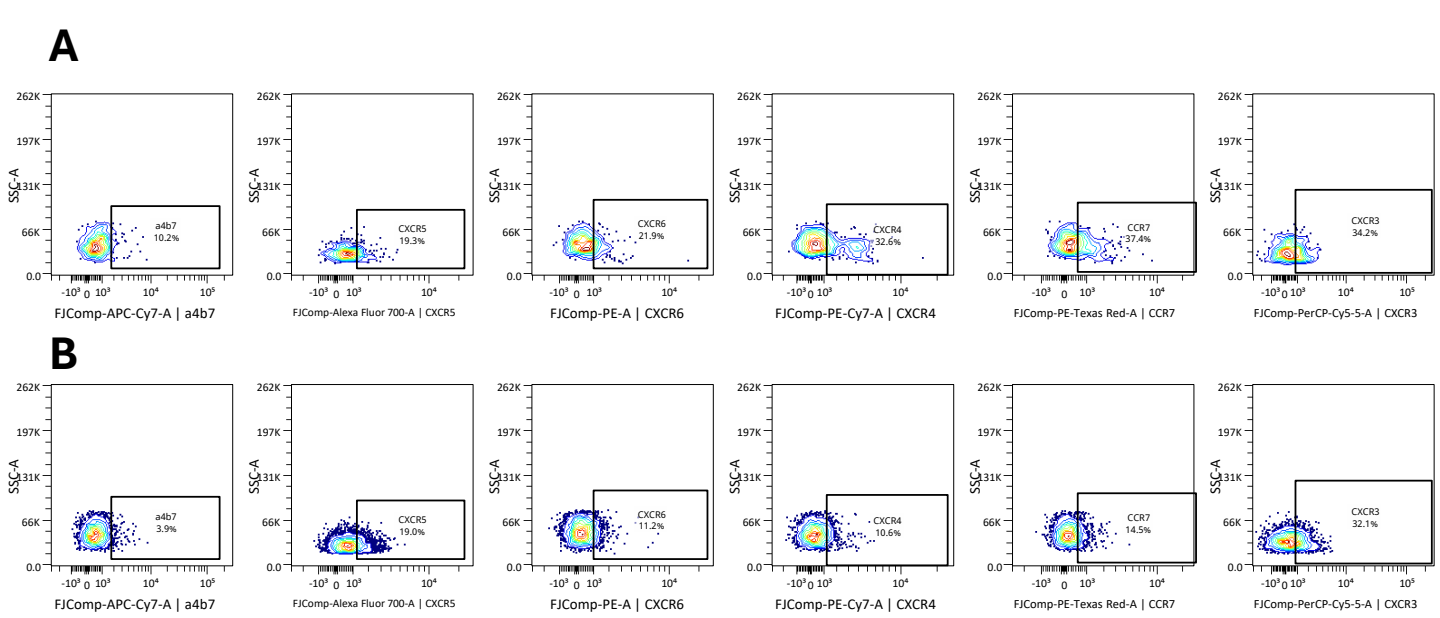


Figure S7. Gating strategy for homing markers on NKG2A^{high} cells (A) and NKG2A^{low} (B).

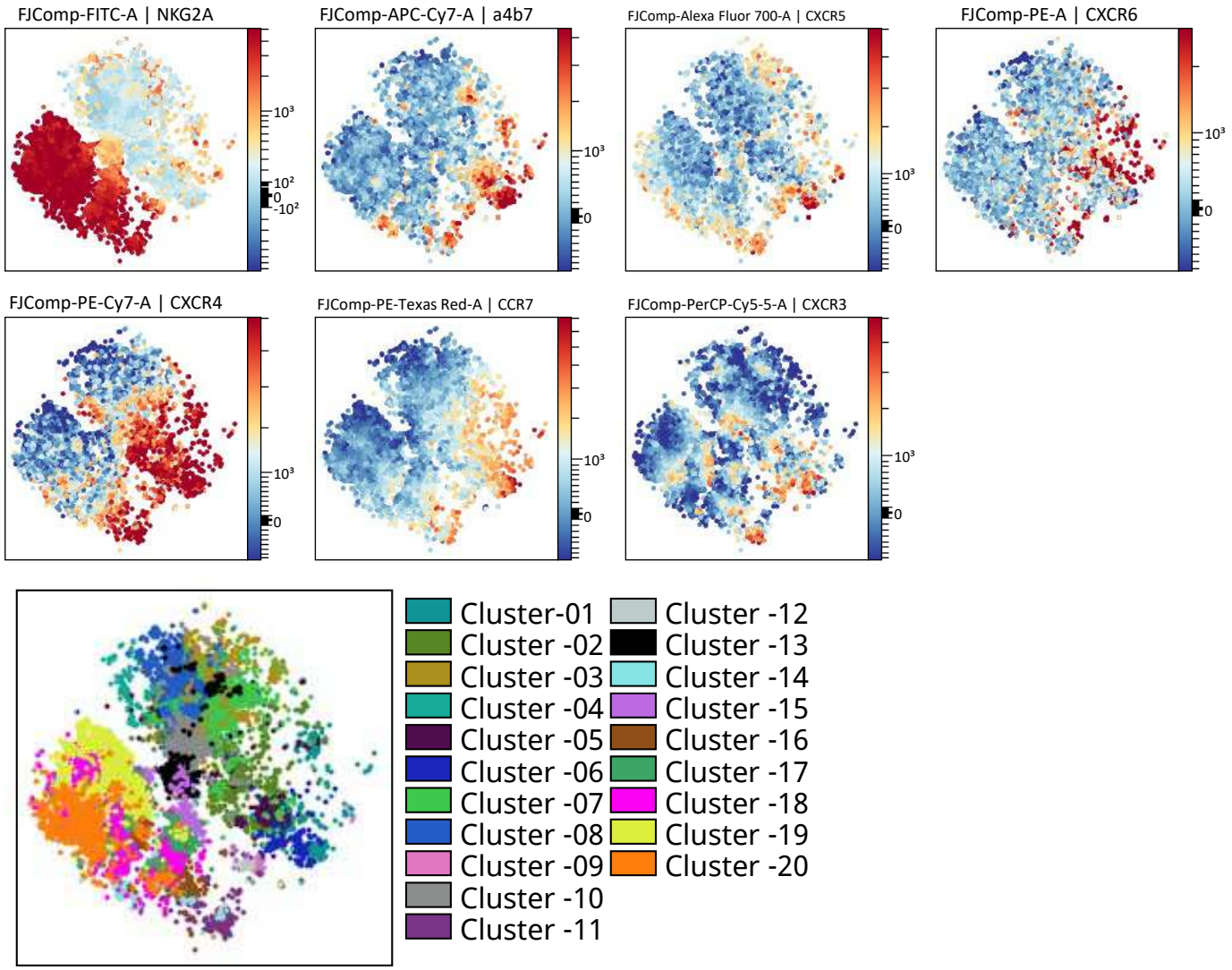


Figure S8. tSNE and expressiong of homing markers in NK cells before ATI.

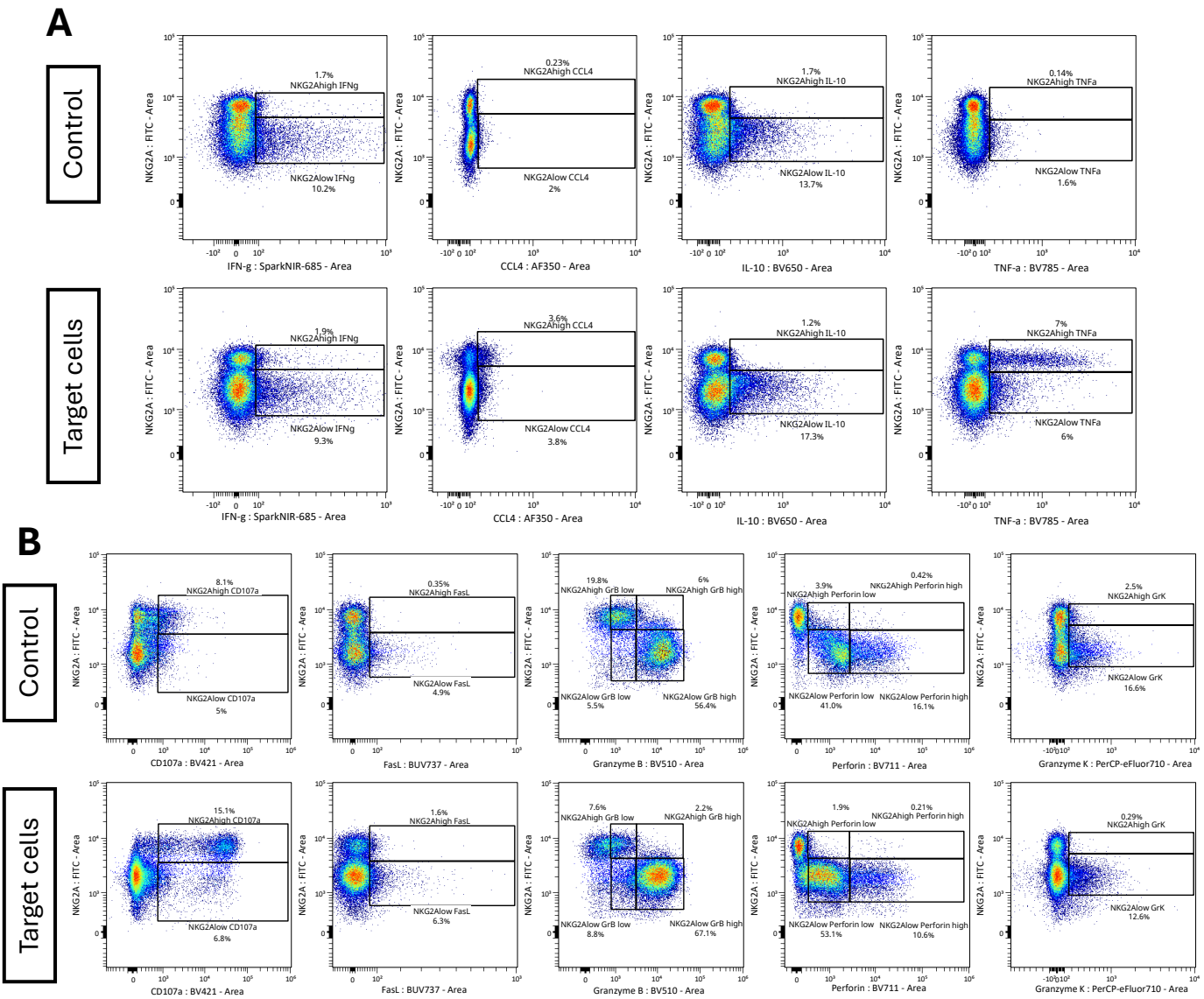


Figure S9. Gating strategy for (A) cytokine and (B) cytotoxic response to target cells regarding NKG2A expression.

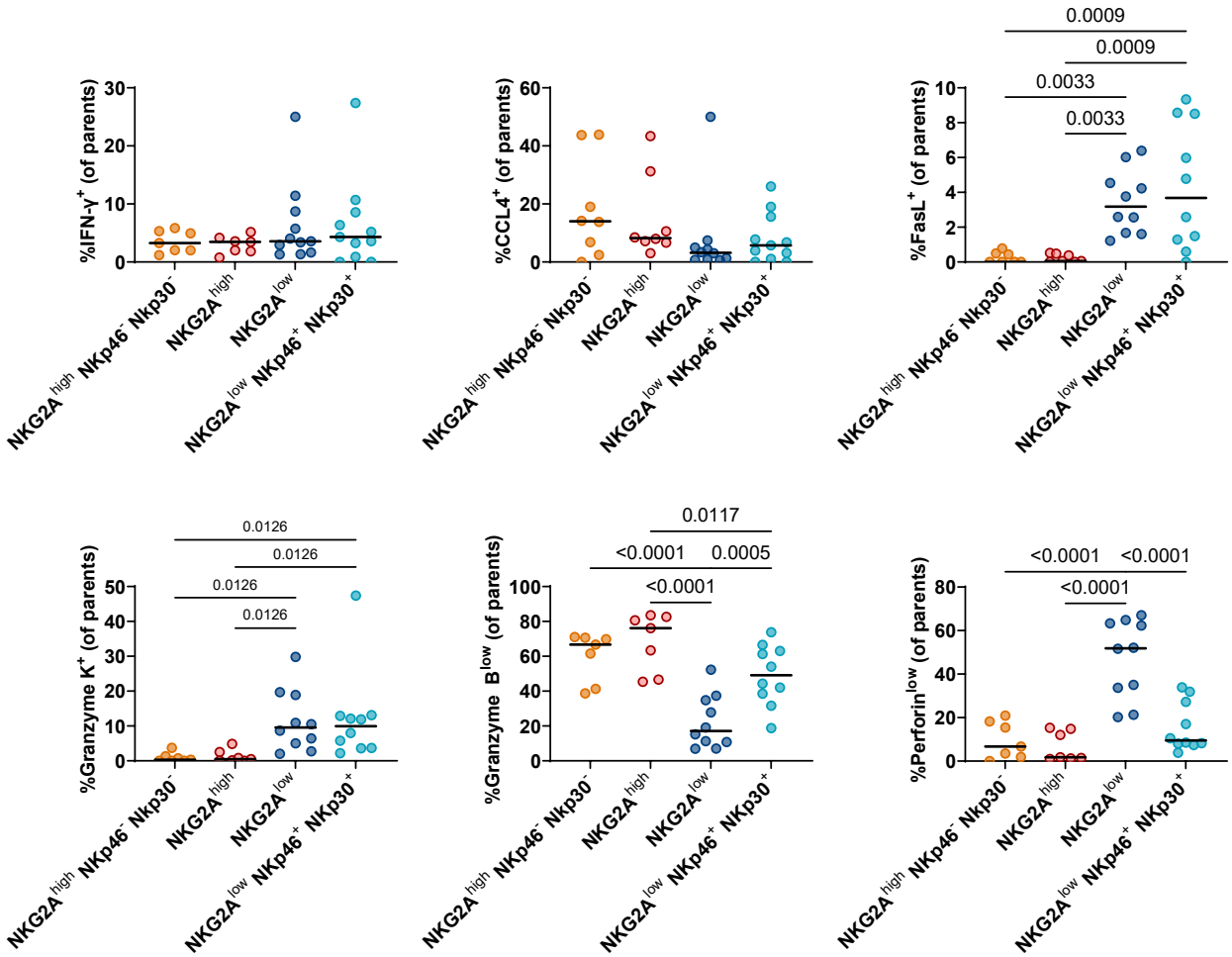


Figure S9. Comparison of IFN-γ (top, left), CCL4 (top, middle), FasL (top, right), Granzyme K (bottom, left) and Granzyme B^{low} (bottom, middle) and Perforinel^{ow} (bottom, right) levels in NKG2A^{high} (red), NKG2A^{high}NKp30^{-}NKp36^{-} (orange), NKG2A^{low} (navy blue) and NKG2A^{low}NKp30^{+}NKp46^{+} (turquoise).